JNeurosci
THE JOURNAL OF NEUROSCIENCE

Research Report: Regular Manuscript

Differential co-assembly of α1-GABA$_A$Rs associated with epileptic encephalopathy

https://doi.org/10.1523/JNEUROSCI.2748-19.2020

Cite as: J. Neurosci 2020; 10.1523/JNEUROSCI.2748-19.2020

Received: 18 November 2019
Revised: 5 May 2020
Accepted: 6 May 2020

Differential co-assembly of α1-GABA$_A$Rs associated with epileptic encephalopathy

Saad Hannan[1*], Aida H. B. Affandi[1], Marielle Minere[1¶], Charlotte Jones[1], Pollyanna Goh[2], Gary Warnes[2], Bernt Popp[3,4], Regina Trollmann[5], Dean Nizetic[2,6] & Trevor G. Smart[1*]

1. Department of Neuroscience, Physiology and Pharmacology, University College London, Gower Street, London WC1E 6BT, UK

2. The Blizard Institute, Barts & The London School of Medicine, Queen Mary University of London, 4 Newark Street, London, E1 2AT, UK

3. Institute of Human Genetics, University Hospital Erlangen, Friedrich-Alexander-Universität Erlangen-Nürnberg (FAU), Schwabachanlage 10, 91054 Erlangen, Germany.

4. Institute of Human Genetics, University of Leipzig Hospitals and Clinics, Leipzig, Germany.

5. Department of Pediatrics, Division of Neuropediatrics, Friedrich-Alexander-Universität Erlangen-Nürnberg (FAU), Erlangen, Germany

6. Lee Kong Chian School of Medicine, Nanyang Technological University, 11 Mandalay Road, 308232 Singapore

*Correspondence to: s.hannan@ucl.ac.uk and t.smart@ucl.ac.uk

Keywords – GABA$_A$ receptors, Epilepsy, Inhibition, Encephalopathy, Cell surface expression, Multi-α GABA$_A$ receptor, α-subunit heteromers

Abbreviated title: GABA$_A$R assembly and epileptic encephalopathy

Number of pages: 31

Number of Figures: 8

Number of Tables: 2

Number of words abstract: 185

Number of words significance statement: 117

Number of words introduction: 319

Number of words discussion: 1500

Number of references: 41

Acknowledgements – TGS and SH are supported by MRC UK, Wellcome Trust and International Rett Syndrome Foundation (3606). DN is supported by the Singapore National Medical Research Council (NMRC/CIRG/1438/ 2015), Singapore Ministry of Education Academic Research Fund Tier 2 grant (2015-T2-1-023) and The Wellcome Trust "LonDownS Consortium" Strategic Funding Award (098330/Z/12/Z) (UK). BP is supported by the Deutsche Forschungsgemeinschaft (DFG) grant PO2366/2–1

¶Current address for Marielle Minere: Max Planck Institute for Metabolism, Gleueler Strasse 50, Cologne, 50931, Germany

Conflict of interest - The authors declare no competing financial interests.

Abstract

$GABA_A$ receptors ($GABA_ARs$) are profoundly important for controlling neuronal excitability. Spontaneous and familial mutations to these receptors feature prominently in excitability disorders and neurodevelopmental deficits following disruption to GABA-mediated inhibition. Recent genotyping of an individual with severe epilepsy and Williams-Beuren Syndrome identified a frameshifting *de novo* variant in a major $GABA_AR$ gene, *GABRA1.* This truncated the α1 subunit between the third and fourth transmembrane domains and introduced 24 new residues forming the mature protein, $α1^{Lys374Serfs*25}$. Cell surface expression of mutant murine $GABA_ARs$ is severely impaired compared to wild-type, due to retention in the endoplasmic reticulum. Mutant receptors were differentially co-expressed with β3, but not with β2 subunits in mammalian cells. Reduced surface expression was reflected by smaller inhibitory postsynaptic currents, which may underlie the induction of seizures. The mutant does not have a dominant negative effect on native neuronal $GABA_AR$ expression since GABA current density was unaffected in hippocampal neurons, even though mutant receptors exhibited limited GABA sensitivity. To date, the underlying mechanism is unique for epileptogenic variants and involves differential β subunit expression of $GABA_AR$ populations, which profoundly affected receptor function and synaptic inhibition.

Significance Statement

$GABA_ARs$ are critical for controlling neural network excitability. They are ubiquitously distributed throughout the brain and their dysfunction underlies many neurological disorders, especially epilepsy. Here we report the characterisation of an α1-$GABA_AR$ variant that results in severe epilepsy. The underlying mechanism is structurally unusual, with the loss of part of the α1 subunit transmembrane domain and part-replacement with nonsense residues. This led to compromised and differential α1-subunit cell surface expression with β subunits resulting in severely reduced synaptic inhibition. Our study reveals that disease-inducing variants can affect $GABA_AR$ structure, and consequently subunit assembly and cell surface expression, critically impacting on the efficacy of synaptic inhibition, a property that will orchestrate the extent and duration of neuronal excitability.

Introduction

γ-Aminobutyric acid (GABA) type-A receptors ($GABA_ARs$) maintain homeostasis over brain excitation by mediating membrane hyperpolarisation and shunting of neuronal excitability (Mitchell and Silver, 2003; Mann and Paulsen, 2007). $GABA_ARs$ are heteropentamers assembled from 19 subunits encoded by 8 gene families: *GABRA1-6*, *GABRB1-3*, *GABRG1-3*, *GABRR1-3*, *GABRD, GABRE, GABRP,* and *GABRQ* (Sieghart and Sperk, 2002). The prototypical $GABA_AR$ is composed of 2α, 2β and a γ or δ subunit with those containing α1 being the most abundant subtype particularly in the cortex where they account for the majority of synaptic $GABA_ARs$ (Hutcheon et al., 2004; Datta et al., 2015). Given their pivotal role in the brain, mutant $GABA_AR$ subunits frequently underlie excitability disorders such as epilepsy (MacDonald et al., 2004; Maljevic et al., 2019).

Recently, an individual with dual pathology of Williams-Beuren Syndrome (WBS) and severe epilepsy was identified (Popp et al., 2016). The neurological phenotypes of WBS are characterised by cognitive and neurodevelopmental impairment, hypotonia, poor balance and coordination (Popp et al., 2016). However, in addition to the WBS-associated microdeletion on chromosome 7, a *de novo* single base deletion c.1200del, p.(Lys401Serfs*25, numbering includes the signal peptide) in the *GABRA1* gene was observed. This caused a frame-shift that removed all residues from Lys374 onwards to the C-terminus of the mature human protein while introducing 24 new amino acids followed by a stop codon ($\alpha1^{Lys374Serfs*25}$; referred to hereafter as $\alpha1^{Mut}$). Thus, the frame-shift prematurely truncates the predominant $GABA_AR$ α subunit in the brain removing part of the M3-M4 loop and the downstream fourth transmembrane (M4) domain and C-terminal.

Given the likely important consequences for inhibitory signalling following a drastic structural change to the α1 subunit, including the insertion of new residues, we have characterised the molecular pharmacological properties of mutant $GABA_ARs$ in heterologous expression systems and neurons using electrophysiology, flow cytometry and imaging. We identify severe impairments to cell surface $GABA_AR$ expression, reduced GABA sensitivity, and unexpected differential effects on receptor assembly.

Materials and methods

Neurological monitoring and Electroencephalography (EEG) – As a result of the intractable epileptic encephalopathy, the individual carrying the variant c.1200del, p.(Lys401Serfs*25) in *GABRA1* was regularly seen at the pediatric neurology clinic (as an out patient) in Erlangen. EEG monitoring was performed by an experienced pediatrician trained in neurophysiology and epileptology using standard investigative practice and established procedures. Informed written consent for publication of this clinical case was obtained from the legal guardians and publication of the updated clinical course is covered by the ethical vote for retrospective translational research studies under the auspices of the Ethical Committee of the Medical Faculty of the Friedrich-Alexander-Universität Erlangen-Nürnberg.

cDNA and molecular biology – cDNAs for wild-type mouse α1, β2, β3, $\beta3^{DNTK}$, γ2L, $\alpha1^{myc}$ and eGFP have been described previously (Taylor et al., 1999; Hannan and Smart, 2018; Hannan et al., 2019). Mouse $\alpha1^{Lys373Serfs*25}$ (equivalent to human $\alpha1^{Lys401Serfs*25}$ with signal sequence; $\alpha1^{Lys374Serfs*25}$ without signal sequence; defined hereafter as $\alpha1^{Mut}$) was created using α1 as template and a single inverse PCR (Hannan et al., 2019) and ligation by removing 54 amino acids after Ser373 of the mature protein and adding 24 amino acids followed by a stop codon using CTAACAGTATCAGCAAAGTTAACAGATTGTCAAGAATAGGTTCTTTTAGTCGTATTCTGTTG as forward and CGGCTTTCTAGGGTTTTGGTGATTTTGCTTTGGTGAGACTTCTTTCGGTTCTATGGTCGCAC as reverse primers. The $\alpha1^{\Delta373}$ subunit cDNA was created using inverse PCR with TAGGTTCTTTTAGTCGTATTCTGTTG as forward and CTTGACTTCTTTCGGTTCTATGGTCGC as reverse primers. The fidelity of all cDNAs was checked using DNA sequencing.

Cell culture – All cell culture reagents were acquired from ThermoFisher unless otherwise stated. HEK-293T cells were grown at 37°C in 95% air/ 5% CO_2 in Dulbecco's modified Eagle's medium (DMEM) supplemented with 10% v/v fetal calf serum (FCS), penicillin-G/ streptomycin (100 u/ ml and 100 µg/ ml) and 2 mM L-glutamine. Cells were seeded on 22 mm glass coverslips coated with poly-L-lysine (Sigma) for confocal imaging and whole cell electrophysiology and in 6 cm adherent cell culture dishes for flow cytometry.

Primary hippocampal neurons – Use of animals conformed to the UK Animals (Scientific Procedures) Act 1986 and relevant European Union directives. Embryonic day 18 (E18) Sprague Dawley rat hippocampi of either sex were dissected in ice-cold Hank's Balanced Salt Solution (HBSS) and dissociated neurons were seeded onto 18 mm glass coverslips

coated with poly-D-lysine (Sigma) in a plating media containing minimum essential media (MEM) supplemented with 5% v/v FCS, 5% v/v horse serum, penicillin-G/ streptomycin (100 u/ ml and 100 µg/ ml), 20 mM glucose (Sigma) and 2 mM L-glutamine. Two hours after seeding, the plating media was removed and replaced with a maintenance media comprising Neurobasal-A with 1% v/v B-27, penicillin-G/ streptomycin (100 u/ml / 100 µg/ml), 0.5% v/v Glutamax and 35 mM glucose. Neurons were grown at 37°C and 95% air /5% CO_2.

Transfection – HEK-293 cells were transfected with cDNAs encoding for eGFP along with wild-type or mutant α1 subunits, with β2/3 and γ2L in equimolar ratios (1:1:1:1) using a calcium chloride method (Hannan and Smart, 2018). Neurons were transfected at 7 days *in vitro (DIV)* with eGFP along with wild-type or mutant α1 subunits in equimolar ratios also using a calcium chloride method (Hannan et al., 2013).

Oocytes and two electrode voltage clamp - *Xenopus laevis* ovaries were removed from frogs *and* incubated for 2-3 hr in collagenase type I (Worthington) in OR2 solution containing (in mM) 85 NaCl, 5 HEPES and 1 $MgCl_2$ (pH 7.6 adjusted with KOH). De-folliculated oocytes were washed in OR2 and maintained at 18°C in Barth's solution containing (in mM): 88 NaCl, 1 KCl, 0.33 $Ca(NO_3)_2$, 0.41 $CaCl_2$, 0.82 $MgSO_4$, 2.4 $NaHCO_3$, and 10 HEPES, pH adjusted to 7.6 with NaOH. Oocytes were injected with 27.6 nl of a 30 ng / µl mix containing wild-type or mutant α1 subunits, β2/3 and γ2L in equimolar ratios (1:1:1) and used for two-electrode voltage clamp (TEVC) recordings 1-2 days after injection.

TEVC recordings were performed at room temperature in a recording solution containing (in mM) 100 NaCl, 2 KCl, 2 $CaCl_2$, 1 $MgCl_2$, and 5 HEPES (pH adjusted to 7.4 with NaOH) using an Axoclamp 2B amplifier, a Digidata 1322A interface and pClamp 8 (Molecular Devices). Oocytes were voltage clamped at -60 mV and current data were digitized at 500 Hz and filtered at 50 Hz. GABA concentration response curves were constructed as described under 'Electrophysiology' below.

Flow cytometry – 48 hr after transfection, HEK-293 cells were washed with HBSS to remove growth media and incubated in trypsin for 30s with gentle tapping to dislodge cells into suspension. The reaction was stopped with serum-containing HEK-293 growth media and after centrifugation the pellet containing the cells was resuspended in ice-cold phosphate buffered saline (PBS; Sigma) supplemented with 10% FCS and 1% sodium azide. From this point onwards all reactions were carried out in the serum containing PBS at 4°C. For labelling cell surface $GABA_A$Rs, cells were centrifuged one more time before resuspension in a rabbit primary antibody against an N-terminal extracellular epitope of the α1 subunit (Abcam Ab 33299) and incubated for 30-45 min under gentle shaking. Cells were washed

twice to remove primary antibodies and then incubated in Alexa-Fluor 647 conjugated anti-rabbit secondary antibody for 30 min under gentle shaking. Cells were washed twice to remove secondary antibodies and immediately transported to the flow cytometry facility for data acquisition.

For measuring the amount of total receptors, cells were harvested and washed to remove media and fixed in 4% paraformaldehyde (PFA) in PBS for 10 min at room temperature under gentle shaking. Cells were washed twice in the serum-containing PBS to remove excess PFA and incubated in 0.1% triton X in PBS for 10 min at room temperature under gentle shaking to permeabilise the membrane. After washing twice, cells were resuspended in a mouse primary antibody against α1 subunits (NeuroMab clone N95/35) and incubated for 30 min at 4°C under gentle shaking. Cells were washed twice to remove primary antibodies and incubated in Alexa-fluor 647 conjugated anti-mouse secondary antibody for 30 min at 4°C under gentle shaking. Cells were washed twice to remove secondary antibodies before flow cytometry.

Flow cytometry was carried out using a BD FACS Aria IIIu fitted with Blue (488 nm), Red (633 nm), Violet (405 nm) and Yellow-Green (561 nm) lasers and FACS Diva software ver 8.0.1 (San Jose, CA). Cells were gated on FSC (Forward Scatter) v SSC (Side Scatter) and cell doublets discriminated by SSC-W parameter. GFP and Alexa Fluor 647 were detected on the Blue laser 530/30 nm and Red laser 660/20 nm parameters using Area.

Based on the auto-fluorescence profiles of untreated or primary and secondary antibody incubated untransfected cells, the levels of background fluorescence were segmented in fluorescence scatter plots of eGFP against Alexa Fluor 647 expression levels of cells. This gave rise to four quadrants: Q1 – Alexa Fluor 647 only, Q2 – eGFP and Alexa Fluor 647, Q3 – auto-fluorescence and Q4 - eGFP only. The median cell surface fluorescence intensity for mutant $GABA_ARs$ in Q2 was normalised to the corresponding median for wild-type $GABA_ARs$ in the same run. In addition, the median %Q2 area or the % of cells in Q2, which is representative of the efficiency of cell surface expression, was normalised to the median %Q2 area for wild-type $GABA_ARs$.

Immunolablling and confocal imaging – 48 hours after transfection, HEK-293 cells and neurons were washed with PBS and fixed in 4% PFA for 10 min at room temperature followed by incubation in primary antibody (mouse anti-myc; Abcam Ab32) in PBS containing 3% FCS at room temperature for 45 min. After washes to remove the primary antibody, cells were incubated in secondary antibody (goat anti-mouse Alexa fluor 555) in PBS containing

3% FCS at room temperature for 30 min. After serial washing, cells were mounted in the antifade agent, ProLong gold.

For permeabilised cells, after fixation, incubation proceeded in 0.1% triton X in PBS containing 10% FCS for 10 min at room temperature followed by serial washes and incubation in primary (mouse anti-α1, Neuromab; rabbit anti calnexin, Ab22595) and secondary (goat anti-mouse Alexa fluor 555; goat anti rabbit 647) antibodies. Cells were mounted in ProLong gold reagent.

Confocal imaging was undertaken using an LSM 510 Meta microscope with a x40 oil immersion objective and a 488 nm laser for imaging eGFP, 543 nm laser for imaging Alexa Fluor 555 and 634 nm laser for imaging Alexa Fluor 647. Cells were imaged sequentially at optimum optical thickness in 8-bit.

Image analysis – Images were analysed using ImageJ (ver 1.52i). Mean cell surface fluorescence levels were measured from defined regions-of-interest around the periphery of cells (Hannan et al., 2013). Colocalisation analysis was undertaken using Just Another Co-localisation Plugin (JACoP) in ImageJ. After applying thresholds, Pearson's coefficient (*r*) between α1 subunit and ER fluorescence values for individual pixels was determined. In addition, the proportion of α1 subunit fluorescence that colocalised with the ER (Manders coefficient M1) and the proportion of ER fluorescence that colocalised with α1 subunits (Mander's coefficient M2) were also measured.

Electrophysiology – Whole-cell electrophysiology of HEK-293 cells was carried out 48 hr after transfection by voltage clamping cells at −30 mV with optimised series resistance (Rs, <10 MΩ) and whole-cell membrane capacitance compensation. Borosilicate glass patch electrodes (resistances of 3 – 5 MΩ) were filled with an internal solution containing (mM): 120 CsCl, 1 $MgCl_2$, 11 EGTA, 30 KOH, 10 HEPES, 1 $CaCl_2$, and 2 K_2ATP; pH – 7.2. Cells were superfused with a saline solution containing (in mM): 140 NaCl, 4.7 KCl, 1.2 $MgCl_2$, 2.52 $CaCl_2$, 11 Glucose, and 5 HEPES; pH 7.4. Membrane currents were filtered at 5 kHz (−3 dB, 6th pole Bessel, 36 dB per octave).

GABA concentration response curves were constructed by measuring GABA-activated currents (*I*) elicited at each GABA concentration and normalising these currents to maximal responses (I_{max}). The concentration response relationship was fitted with the Hill equation:

$$I/I_{max} = (1 / (1 + (EC_{50}/[A])^n)$$

where A is the concentration of GABA, EC_{50} is the concentration of GABA giving 50% of the maximum response and n is the Hill slope.

The kinetics of GABA-activated currents in HEK-293 cells was studied by applying 1 mM GABA (for wild-type receptors) and 100 mM GABA (for mutant receptors) via a modified U-tube (Thomas and Smart, 2012). The activation rate was estimated by measuring the time taken to ascend 20 - 80% of I_{max} during GABA application. The deactivation rate was estimated by fitting a single exponential function from the point when GABA application ceased until the baseline was reached.

Neurons transfected at *7 DIV* with wild-type or mutant α1 subunit cDNAs were voltage clamped at –60 mV for recording GABA-activated currents or spontaneous inhibitory postsynaptic currents (sIPSCs) at 12-14 *DIV*. Neurons were superfused with the same saline solution as used for HEK-293 cells but containing 2 mM kynurenic acid to block excitatory neurotransmission. Membrane capacitance was measured by applying brief -10 mV pulses to hyperpolarise the membrane and calculating the area under the capacity current discharge curve. Current densities were measured by dividing maximal GABA currents obtained with 1 mM GABA at -20 mV holding potential with the membrane capacitance. Cumulative probability distributions of sIPSC amplitudes and areas mediated by wild-type and mutant receptors were compared using non-parametric statistics, whereas mean sIPSC frequency, T_{50} and decay τ were compared by using parametric tests.

Modelling GABA concentration response curves – To predict the GABA concentration response curves for a varying mixture of sub-populations of $GABA_A$Rs containing either only $\alpha1^{WT}$ or $\alpha1^{Mut}$ subunits, or a binomial mixture of both, with β3 and γ2L subunits, we devised the following modified Hill equation:

$$I_{GABA} = \left[\frac{[A]}{[A] + EC_{50}1}\right]^{i} u * n + \left[\frac{[A]}{[A] + EC_{50}2}\right]^{j} v * m + \left[\frac{[A]}{[A] + EC_{50}3}\right]^{k} w * p$$

Where the GABA current (I_{GABA}) compared to the maximal response for each GABA concentration ([A]) is determined by up to three populations of $GABA_A$Rs expressed with relative proportions of n, m and p (where m + n + p =1) and trafficking factors u, v and w, where a value of 1 signifies efficient near-complete expression at the cell surface and 0 no surface expression. $EC_{50}1$, $EC_{50}2$ and $EC_{50}3$ represent the concentrations of GABA evoking 50% of the maximal GABA response for $\alpha1^{WT}$, $\alpha1^{WT}$+ $\alpha1^{Mut}$, and $\alpha1^{Mut}$ respectively. The symbols, i, j and k represent the Hill slope factors. For single populations of $GABA_A$Rs the

conventional Hill equation was used to provide curve fits to the GABA concentration response data:

$$I_{GABA} = \left[\frac{[A]^i}{[A]^i + EC50^i}\right]$$

where the symbols are as previously defined.

Non-stationary noise analysis – For peak-scaled non-stationary variance analysis, synaptic GABA currents were individually selected for clean rise and decay phases i.e. lacking inflections, secondary peaks, or current artefacts. The clean synaptic currents were imported into WinWCP v5.2.3 (John Dempster, University of Strathclyde, Glasgow), and the peak of the averaged sIPSCs was aligned to the negative rise phase and peaks of the individual sIPSCs chosen for the analysis. The decay phases of individual sIPSCs were subtracted from the mean sIPSC decay to generate the sIPSC variance which was plotted against the corresponding mean current according to the parabolic function:

$$\sigma^2 = [i.I_{m-}(I_m^2/N)] + Var_b$$

Where σ^2 is the current variance, i represents single channel current, I_m is the mean current and N is the average number of synaptic receptors activated during an sIPSC. Var_b represents the baseline current variance. This equation was used to generate fits to the current variance – mean plots and to estimate i and N for synaptic $GABA_A$Rs.

Experimental design and statistics - All statistical tests that have been used, and applied to sample sizes in the study, are indicated in the figure legends and results section. For parametric data, two groups were compared using two-tailed Student's t-test. For comparing data from three or more groups, a one-way ANOVA was used (GraphPad Instat 3). Where normality in the data spread was not apparent, we used non parametric tests in conjunction with SPSS (ver 24). Data in the bar charts represent means ± standard error of means (s.e.m). Data in box plots show 25 – 75 % interquartile ranges (IQRs) and the median.

Results

Severe epileptic encephalopathy with mutant $GABA_ARs$. The patient's clinical characteristics up to the age of 14 months have been reported previously when the variant c.1200del, p.(Lys401Serfs*25) in *GABRA1* and the common microdeletion in 7q11.23 were identified as the genetic cause of the phenotype, including refractory epileptic encephalopathy and characteristic features of WBS (Popp et al., 2016). Since that period, the patient's anticonvulsant therapy has been regularly optimised. Repeated EEG analyses confirmed severe epileptic encephalopathy with slow background activity and diffuse epileptic discharges. At age 38 months, epileptic episodes were characterized by daily myoclonic seizures and rare short-tonic seizures lasting 30 – 60 s. Global neurodevelopmental deficits, including hypotonic-ataxic cerebral palsy and severe intellectual disability were also evident.

The physiological consequences of the genetic variation were probed by generating an equivalent mouse α1 subunit replicating the truncation in the human subunit starting from lysine 373 of the mature α1 protein (equivalent to human Lys374), followed by the addition of 24 *de novo* residues that are found in the WBS individual (designated as $\alpha1^{Mut}$; Fig. 1*A*). In addition, a truncation mutant from Lys373 that excluded the frame-shift was also created to examine the effect of the 24 additional new residues (designated as $\alpha1^{\Delta373}$; Fig. *1A*) on $GABA_AR$ function.

A majority of α1-$GABA_ARs$ are co-assembled with β2/β3 and γ2L subunits in the brain (Whiting, 2003). Thus, GABA sensitivity of $\alpha1^{Mut}$ was studied in isolation in HEK-293 cells co-expressed with either, β2 or β3 subunits, and γ2L. Receptors comprising $\alpha1^{Mut}\beta3\gamma2L$ and $\alpha1^{\Delta373}\beta3\gamma2L$ receptors were considerably less sensitive to GABA ($F_{(2,16)}$ = 8.491, p = 0.0031, One-way ANOVA, *Table 1*; Fig. 1*B-C*) and with lower maximal currents ($F_{(2,23)}$ = 61.823, P<0.001, One-way ANOVA; Fig. 1*B-C*). There was no difference (p = 0.918, p = 0.986, respectively, Tukey-Kramer post-hoc test) between the two mutants suggesting that the additional 24 amino acids do not additionally affect GABA potency and/or receptor activation. Of note, both mutant receptors failed to activate in response to 100 mM GABA when assembled with β2 subunits ($\alpha1^{Mut}\beta2\gamma2L$ and $\alpha1^{\Delta373}\beta2\gamma2L$) highlighting the importance of the β subunit for assembly, trafficking and/or signalling of $\alpha1^{Mut}$-containing heteromers in mammalian cells.

Receptor activation, desensitisation and deactivation of recombinant $\alpha1^{Mut}\beta3\gamma2L$ and $\alpha1^{\Delta373}\beta3\gamma2L$ were studied by applying maximal GABA concentrations (1 mM for WT and 100 mM for each mutant). Both mutant receptors displayed slower activation (p = 0.0025) and

deactivation (p = 0.0171) kinetics compared to WT receptors (Fig. 1*D*) suggesting a profound defect(s) in gating and/or GABA binding. Moreover, neither mutant showed evidence of macroscopic desensitisation (Fig. 1*D*). These results indicated that adding 24 new amino acids to the α1 subunit did not alter the signalling properties of mutant receptors in comparison to the truncated form of the receptor.

To further assess the differential expression profile of $\alpha1^{Mut}$ with β2 and β3 subunits, we reverted to an amphibian expression system that permits the expression of a wider range of constructs compared to mammalian cells (Hanrahan, 2004) and also enables longer cell incubation times to resolve slower rates of receptor expression (Smart and Krishek, 2003), which may be missed in HEK cells. As noted with HEK-293 cell expression, both the sensitivity to GABA (P<0.001; Fig. 2*A*-*C*) and maximal GABA current (p = 0.0382; Fig. 2*A, D*) for $\alpha1^{Mut}\beta3\gamma2L$ were reduced compared to WT receptors when expressed in *Xenopus* oocytes. However, in contrast to HEK cells, $\alpha1^{Mut}\beta2\gamma2L$ were also expressed in oocytes to a similar extent to β3-containing receptors. GABA sensitivity (p = 0.0015) was reduced together with lowered maximal currents (p = 0.0003, Fig. 2*A*-*D*). These results confirmed the impaired GABA activation, gating and GABA sensitivity of the mutant receptors and provided the first evidence that their expression and signalling properties depended upon co-assembly and/ or trafficking with different β subunits in mammalian cells.

Impaired cell surface expression of mutant α1-$GABA_A$Rs. Reduced GABA-activated currents for mutant receptors and the absence of current for β2-containing mutant receptors in mammalian cells could reflect reduced cell surface expression. We studied this aspect using live HEK-293 cells expressing either, $\alpha1^{WT}$, $\alpha1^{Mut}$ or $\alpha1^{\Delta373}$ alongside β2 or β3, and γ2L subunits. Surface expression was determined by flow cytometry in conjunction with an N-terminal α1 subunit antibody. With β2 and γ2L subunits a substantive decrease in surface expression (>94-95%; $F_{(4,28)}$ = 74.010, P<0.001, One-way ANOVA) was evident for $\alpha1^{Mut}$ and $\alpha1^{\Delta373}$, compared to $\alpha1^{WT}$ and eGFP controls (*Table 2;* Fig. 3*A*-*B*). Similarly, α1 mutant or truncated receptors also exhibited reduced ($F_{(4,24)}$ = 115.331, P<0.001, One-way ANOVA) cell surface expression when co-assembled with β3 and γ2L (Fig. 3*A,C*). Although 5-fold more receptors reached the cell surface with β3 compared to β2 subunits, surface expression was still severely impaired compared to WT controls ($F_{(4,24)}$ = 314.885, P<0.001, One-way ANOVA; Fig. 3*A,C*). Interestingly, the efficiency of expression was lower (p=0.02, Tukey-Kramer post-hoc test) for $\alpha1^{Mut}\beta3\gamma2L$ compared to $\alpha1^{\Delta373}\beta3\gamma2L$, suggesting that the additional 24 new amino acids affected subunit assembly and/ or cell surface trafficking, a feature that was not apparent for β2-containing mutant receptors.

To discount the possibility that variable total receptor levels affected cell surface expression, flow cytometry was used to measure total (intracellular and surface) subunit levels in permeabilised cells expressing mutant and WT α1 subunits, with either β2 ($F_{(3,16)}$ = 255.156 (fluorescence)/ 54.140 (efficiency), P<0.001, One-way ANOVA) or β3 subunits ($F_{(3,16)}$ = 166.694 (fluorescence)/ 21.825 (efficiency), P<0.001, One-way ANOVA), and γ2L subunits. No differences (P>0.05, Tukey-Kramer post-hoc) in fluorescence intensities or expression efficiencies were observed between WT and mutant receptors (Fig. 3*D-F*) suggesting impaired cell surface expression of mutant receptors does not reflect intracellular expression levels.

To corroborate the flow cytometry results, we used immunocytochemistry and confocal imaging of $GABA_A$Rs expressed in HEK-293 cells by targeting the γ2L subunit with an N-terminal antibody. This also revealed reduced surface expression of $\alpha1^{Mut}$ with β3γ2L-containing receptors and a near-complete loss of surface labelling for $\alpha1^{Mut}$ with β2γ2L-containing receptors (*data not shown*). Overall, these results demonstrate a severe reduction of cell surface expression of $\alpha1^{Mut}$ containing receptors that depends on the co-assembled β subunit with only β3 supporting a severely limited surface expression of mutant $GABA_A$Rs in HEK-293 cells.

To explore which unique motifs in the β3 subunit enable co-assembly with mutant α1 subunits, we selected a conserved stretch of amino acids in the extracellular domain (ECD) previously shown to affect homomeric β subunit assembly. Substitution of the β3 GKER assembly box sequence to DNTK, found in β2 subunits (Taylor et al., 1999), reduced ($F_{(4,10)}$ = 316.991, P<0.001, One-way ANOVA; p=0.016 Tukey-Kramer post-hoc test compared to $\alpha1^{Mut}$; Fig 4*A-B*) but did not abolish cell surface expression of β3 subunits (p=0.001 compared to eGFP controls; Fig 4*A-B*). This suggests that the GKER motif in conjunction with other domains, including the TMDs and intracellular linkers, are important for the differential cell surface expression of $\alpha1^{Mut}$ with β3 subunits.

The effect of the frame-shift on α1-$GABA_A$R cell surface levels was also studied in hippocampal neurons expressing either N-terminal myc-tagged $\alpha1^{WT}$ or $\alpha1^{Mut}$ subunits, and utilising co-assembly with native β and γ2L subunits. The myc-tag did not affect α1 subunit receptor sensitivity to GABA (p = 0.8303; Fig. 4*C-D*). Immunolabelling with anti-myc antibodies in non-permeabilised neurons revealed clear cell surface staining for myc-tagged $\alpha1^{WT}$ subunits. However, expression of myc-tagged $\alpha1^{Mut}$ was significantly compromised (P<0.001, one-way ANOVA) but higher than background eGFP-only fluorescence levels

(P<0.01, one-way ANOVA) (Fig. 4*E-F*). Thus, impaired cell surface expression of mutant α1-$GABA_A$Rs was also apparent in hippocampal neurons.

Intracellular retention of mutant α1 subunits. To investigate whether mutant receptors were retained intracellularly, their co-localisation with the endoplasmic reticulum (ER) marker calnexin (Leach and Williams, 2011) was studied in HEK-293 cells. As expected, WT α1 subunits were retained in the ER when expressed alone (Connolly et al., 1996). High co-localisation between the α1 fluorophore and ER marker was signified by Pearson's regression (*r*) coefficient, and by Mander's M1 (fraction of α1 that colocalises with calnexin) and M2 coefficients (fraction of calnexin that colocalises with α1) (Fig 5*A-B*). By contrast, WT receptors, expressed with β2/3γ2L, had lower Pearson's *r* ($F_{(5,118)}$ = 120.349, P<0.001, one-way ANOVA), Mander's M1 ($F_{(5,117)}$ = 46.992, P<0.001) and M2 ($F_{(5,120)}$ = 244.694, P<0.001) compared to α1 alone since WT heteromers exited the ER and were expressed at the cell surface.

For $\alpha1^{Mut}$β2/3γ2L receptors, increased ER retention was evident from the high Pearson's *r* and Mander's M1, M2 coefficients. These were near-identical to values determined for α1 alone (p=0.061 - p=0.990 Tukey-Kramer post-hoc test) and significantly higher than those for WT α1β2/3γ2L receptors (p=0.048 - p<0.001, Tukey-Kramer post-hoc test; Fig. 5*A-B*). Thus, ER retention of $\alpha1^{Mut}$ impairs the cell surface expression of $GABA_A$Rs.

Epilepsy-inducing $\alpha1^{Mut}$ impairs GABAergic neurotransmission. To investigate the effect of $\alpha1^{Mut}$ on inhibitory transmission, we expressed $\alpha1^{WT}$ or $\alpha1^{Mut}$ subunits in hippocampal neurons at 7 *DIV* and studied spontaneous inhibitory postsynaptic currents (sIPSCs) at 12-16 *DIV*. For $\alpha1^{Mut}$-expressing neurons, sIPSC amplitudes were reduced (median $\alpha1^{WT}$, -63.4 pA, n = 5664 events from 24 cells; median $\alpha1^{Mut}$, -46.5 pA, n = 5236 events from 25 cells; p<0.001, Mann-Whitney test; Fig. 6*A-B*) without changing sIPSC frequency ($\alpha1^{WT}$, 1.6 ± 0.3 Hz; n = 24; $\alpha1^{Mut}$, 1.1 ± 0.2 Hz; n = 25 cells; p = 0.1220, two-tailed unpaired t test).

The sIPSC kinetics were also altered with the half-decay time (T_{50}) increased for the α1 mutation ($\alpha1^{WT}$, 17.7 ± 1.5 ms, n = 21 cells; $\alpha1^{Mut}$, 26.2 ± 2 ms, n = 24; p = 0.0016, two-tailed unpaired t test) and the mean exponential decay time (τ) also increased ($\alpha1^{WT}$, 23.6 ± 2.3 ms; $\alpha1^{Mut}$, 37.5 ± 2.5 ms, n = 21 - 24; p = 0.0002, two-tailed unpaired t test). As a result of changes to sIPSC amplitudes and decay times, the charge transfer (median $\alpha1^{WT}$, -3221.5 pA.ms, n = 1306; $\alpha1^{Mut}$, -2817 pA.ms, n = 1330; P<0.001; Mann-Whitney test) was reduced

for the $\alpha1^{Mut}$. By comparison, the sIPSC rise-times ($\alpha1^{WT}$, 1.5 ± 0.1 ms, n = 21; $\alpha1^{Mut}$, 1.6 ± 0.1 ms, n = 24; p = 0.7054, two-tailed unpaired t test) remained unaffected.

Reduced sIPSC amplitudes could be due to several factors, including a dominant inhibitory effect of $\alpha1^{Mut}$ on the expression of WT $GABA_AR$ subunits as noted for other epilepsy-inducing mutations of $GABA_ARs$ (Kang et al., 2009). However, maximal GABA-induced current densities were similar for hippocampal neurons expressing $\alpha1^{WT}$ or $\alpha1^{Mut}$ $GABA_ARs$ ($\alpha1^{WT}$: -71.6 ± 5.1 pA/pF, n = 45; $\alpha1^{Mut}$: -62 ± 3 pA/pF, n = 41; p = 0.1196, two-tailed unpaired t test; Fig. 6*C-D*) suggesting that overall cell surface expression *per se* of endogenous $GABA_AR$ subunits remained affected by $\alpha1^{Mut}$. Nevertheless, using non-stationary noise analysis of peak-scaled sIPSCs, the mean number of α1-mutant $GABA_ARs$ activated at inhibitory synapses during the peak of the sIPSCs, compared to $\alpha1^{WT}$ neurons, was reduced (Fig. 6*E-F*; $\alpha1^{WT}$ 100.8 ± 20.3, n = 11; $\alpha1^{Mut}$ 44.2 ± 7.3, n = 9; p = 0.0269, two-tailed unpaired t test) without changing the single channel conductance of synaptic $GABA_ARs$ ($\alpha1^{WT}$ 32.1 ± 8.5 pS, n = 11; $\alpha1^{Mut}$ 38.7± 8.7 pS, n = 9; p = 0.5970, two-tailed unpaired t test). Together, these results suggest that at the cell surface, specifically inhibitory synaptic membranes, $\alpha1^{Mut}$ directly affects receptor numbers and thus synaptic inhibitory current.

Evidence for α1-heteromeric $GABA_ARs$. The impact of the α1 mutation on cell surface $GABA_AR$ expression is most likely reflected by the sizeable reduction in sIPSC amplitude. However, the increased sIPSC decay constants indicated that the mutation was also affecting receptor kinetics. We initially examined whether these effects may be caused by α1 mutant subunits forming a pure population ($\alpha1^{Mut}\beta3\gamma2L$) contrasting with WT α1 subunits expressed ($\alpha1^{WT}\beta3\gamma2L$) in separate pentamers. HEK-293 cells were transfected with cDNAs for $\alpha1^{WT}$ and/or $\alpha1^{Mut}$ (in equal ratio) with β3 and γ2L and the resulting properties of the assembled receptors examined. Our initial premise was that hetero-α1 subunit receptors might not form. Plotting the GABA concentration response data and implementing Hill equation curve fits revealed four outcomes: the expected pure α1-WT and pure α1-Mutant curves for HEK cells expressing separate $GABA_ARs$, and two relationships for cells expressing both $\alpha1^{WT}$ and $\alpha1^{Mut}$ with β3γ2L (Fig. 7*A-C*). For the latter, GABA potency was reduced 9-fold in ~11% of cells (EC_{50} = 87.3 ± 19 μM, n = 5; WT EC_{50} = 10.4 ± 1.7 μM, n = 14, $F_{(2, 57)}$ = 92.344, P<0.001, one-way ANOVA, P<0.001 post-hoc Tukey-Kramer test, Fig. 7*A-C*; arbitrarily designated as type 2) whereas the remainder had indistinguishable EC_{50}s from WT (EC_{50} = 8 ± 0.8 μM, n = 41; p=0.796, Tukey-Kramer test, Fig. 7*A-C*; called type 1). Moreover, the potency of Type 2 cells was lower compared to Type 1 cells (P<0.001, Tukey-Kramer test).

The increased GABA EC_{50} in 11% of cells (type 2) could represent the incorporation of $\alpha1^{Mut}$ into the same pentameric receptor with $\alpha1^{WT}$ and β3γ2L subunits, especially given the different EC_{50}s (Fig. 7*A*-*B*), or conceivably, may reflect changes to the relative cell surface expression levels for pure pentamers of $\alpha1^{WT}$β3γ2L and $\alpha1^{Mut}$β3γ2L.

To investigate whether the latter scenario could account for the change in GABA EC_{50}, we generated theoretical GABA concentration response curves for pure α1-WT and α1-Mutant receptor populations, assuming differential expression levels between 0 and 100%, with a maximum current set to 10% for $\alpha1^{Mut}$ compared to $\alpha1^{WT}$ receptors, and with EC_{50}s for $\alpha1^{Mut}$ and $\alpha1^{WT}$ taken from Figure 1. We explored varying the ratio of $\alpha1^{WT}$ to $\alpha1^{Mut}$ $GABA_A$Rs (keeping the total population constant) and normalising the curves to the maximum response evoked by 50 mM GABA (Fig. 7*D*). Changing the proportion of $\alpha1^{WT}$ to $\alpha1^{Mut}$ between 0 and 100% revealed a family of curves with clear inflections especially when $\alpha1^{Mut}$ was the predominant receptor subunit (Fig. 7*D*), which became difficult to resolve when levels of $\alpha1^{WT}$ were increased (e.g. 50 %).

To match the experimental (Type 2) EC_{50} of 87 μM for the $\alpha1^{WT}\alpha1^{Mut}$β3γ2L receptors, observed in 11% of cells, required a ~10:90% ratio of $\alpha1^{WT}$:$\alpha1^{Mut}$. This seems unrealistic given that only 10% of mutant receptors reach the cell surface and even if this occurred the theoretical curves were clearly biphasic (green line, Fig. 7*D*), a feature not observed experimentally (Fig. 7*C*). Thus determining one EC_{50} for the curve was inappropriate when two obvious components were present.

Given the mismatch of these simulations with the experimental data, we discarded the premise of pure α1-subunit receptor populations and permitted co-assembly of α subunits according to a binomial process. Simulated GABA concentration response curves were generated initially based on a modified Hill equation (see Methods) and the presence of $\alpha1^{WT}$β3γ2L, $\alpha1^{WT}\alpha1^{Mut}$β3γ2L and $\alpha1^{Mut}$β3γ2L in approximate binomial proportions of 0.25: 0.5: 0.25. On this basis, the simulated curves accurately reflected the experimental data and predicted that the majority of receptors at the cell surface were $\alpha1^{WT}$-containing (54%), $\alpha1^{WT}\alpha1^{Mut}$-containing (40%), with the remainder (~6%) just $\alpha1^{Mut}$-containing. Furthermore, on the simulated curves for the $\alpha1^{WT}\alpha1^{Mut}$-containing receptors (blue line and arrow, Fig. 7*E*) an inflection is discernible although this is hard to resolve in the experimental graphs without further data points, but it is a consequence of some pure $\alpha1^{Mut}$-containing receptors accessing the cell surface.

Thus, differential assembly and altered trafficking for the $\alpha1^{Mut}$ receptor will have an impact on the GABA concentration response curves. Moreover, using confocal microscopy, the

levels of cell expression of wild-type receptors do not change when co-expressed with mutant receptors (normalised surface expression levels - $\alpha1^{WT}$ – 100, n = 38; $\alpha1^{WT}$ + $\alpha1^{Mut}$ – 96.4 ± 3.2, n = 42; eGFP only – 1.5 ± 0.5, n = 24. $F_{(2,101)}$ = 355.948, P<0.001, One-way ANOVA; p=0.553 Tukey-Kramer post-hoc wild-type vs wild-type and mutant receptors, Fig 8*A-B*). Taken together, the most likely explanation for the change of GABA-sensitivity in some HEK-293 cells is the incorporation of $\alpha1^{Mut}$ into the same pentameric complex with α1 subunits forming an α-subunit hetero-pentamer with altered kinetic profile.

To explore the importance of the α1 subunit for synaptic inhibition we used the imidazopyridine z-drug, zolpidem, which at 100 nM is a selective-modulator of α1 subunit-containing $GABA_A$ receptors (Pritchett et al., 1989; Perrais and Ropert, 1999). Application of 100 nM zolpidem to neurons expressing $\alpha1^{WT}$ revealed prolongations of sIPSC decays as expected (Vicini et al., 2001), increasing both the T_{50} (p = 0.0094) and exponential decay τ (p = 0.003, Fig. 8*C, D*). Comparing this outcome to neurons expressing $\alpha1^{Mut}$-$GABA_A$Rs revealed two notable features. The sIPSC decay was prolonged (T_{50} and decay τ both P<0.001, Fig. 8*C, E*), but not to the same extent as for $\alpha1^{WT}$ (56 – 65 % increase in T_{50} and τ for $\alpha1^{WT}$, and 28 – 35 % for $\alpha1^{Mut}$). Given that the truncation of the α1 subunit is unlikely to directly affect modulation of the receptor by zolpidem, the difference in sIPSC decay prolongations suggests α1 subunit $GABA_A$Rs are reduced in number at inhibitory synapses.

Overall, these results suggest that α1-mutant containing $GABA_A$Rs are disrupting the expression of $GABA_A$Rs at inhibitory synapses.

Discussion

The advent of high-throughput sequencing heralds a new era for investigating the genetic basis of neurodevelopmental disorders. Whole exome sequencing has identified numerous mutations to genes encoding for ion channels and neurotransmitter receptors that underlie neurological disorders (Foo et al., 2012). To understand how individual variants orchestrate pathological features requires extensive neurobiological and biophysical characterisation of ion channel and receptor dysfunction.

Genetic variants account for over 40% of all epilepsies (Robinson and Gardiner, 2000) and structural modifications to several $GABA_A$R subunits, ranging from residue substitutions to substantive deletions and truncations, with or without frame-shift insertions, alter many aspects of inhibitory signalling including: GABA sensitivity (Hernandez et al., 2016), receptor

activation /deactivation kinetics (Audenaert et al., 2006; Lachance-Touchette et al., 2011; Hernandez et al., 2016; Audenaert et al., 2006; Lachance-Touchette et al., 2011; Hernandez et al., 2016), sensitivity to ligands (Audenaert et al., 2006), ER retention (Kang and Macdonald, 2004; Lachance-Touchette et al., 2011), receptor degradation (Kang et al., 2015), assembly (Hales et al., 2005), and cell surface trafficking/ expression (Sancar and Czajkowski, 2004; Maljevic et al., 2006; Tian et al., 2013). All these features can contribute towards a catalogue of generalised and partial seizures. For example, point mutations affecting α1 subunits associated with epilepsy variously reduce cell surface expression due to nonsense-mediated mRNA decay and ER-associated protein degradation (Gallagher et al., 2005; Kang and Macdonald, 2009). This can alter receptor kinetics and affect GABA sensitivity (Fisher, 2004; Galanopoulou, 2010). These changes can reduce inhibitory synaptic efficacy and reflect the importance of dysfunctional GABA signalling as a key mechanism in genetic epilepsy.

By characterising a variant in the $GABA_AR$ α1-subunit that causes severe epilepsy, we have identified impaired signalling and cell surface expression of $GABA_ARs$ that are unusual in regard to epilepsy. At a molecular level, even though the mutant α1 subunit lacks a substantive structural component, including part of the M3 - M4 domain and all of M4, the mutant receptor still retains its signalling ability, albeit reduced, compared to WT receptors. The large reduction in GABA sensitivity (>400 fold) and maximal currents, including decreased receptor activation and slower deactivation, and reduced synaptic numbers of $GABA_A$ receptors, will all reduce the efficacy of inhibition imparted by this important subpopulation of synaptic $GABA_ARs$ (Galanopoulou, 2010). The combined effects of these defects masked the reduced desensitisation we observed for the mutant, and also reduced charge transfer via synaptic $GABA_ARs$.

The role of M4 is clearly important, but its loss does not prevent $\alpha1^{Mut}$ assembly into the receptor. However, it does influence αβ subunit incorporation. Our experiments using mammalian cells demonstrate that the truncated subunit preferentially associates with β3 over β2 subunits. In regard to their structure, β subunits are very highly conserved (Taylor et al., 2000; Sigel and Steinmann, 2012). Differential assembly and/ or trafficking of the α1 mutants with β subunits might occur because losing M4 may alter α subunit conformation such that there is simply preferred assembly and/ or cell surface trafficking with β3 over β2 subunits. It is clear that the GKER motif in the ECD of β3 subunits is important for enabling expression of $\alpha1^{Mut}$ containing receptors, but given that it has only a partial effect, it indicates that other domains in the β3 subunit must also play important roles. The truncated portion of the α1-mutant subunit's large intracellular domain between M3 and M4 is unlikely to be

559 directly important for this process as substituting the entire domain for a serine-glycine linker,
560 or a *Gloeobacter violaceus* heptapeptide, affected neither the assembly, cell surface
561 expression, nor dramatically affected signalling of α1 with β2 subunits (Jansen et al., 2008;
562 Hannan and Smart, 2018). The preference of $\alpha1^{Mut}$ for β3 over β2 is subtle since assembly
563 in *Xenopus* oocytes is seemingly unaffected by the loss of M4. This suggests that $\alpha1^{Mut}$ and
564 β2 co-assembly is slow and possibly inefficient requiring longer incubation times that are
565 afforded by using *Xenopus* oocytes compared to HEK cells. This highlights the importance of
566 studying disease variants in mammalian, preferably native, systems. Whether the mutation
567 affects cell surface trafficking and/ or subunit co-assembly may be determined from applying
568 biochemical methods. Nevertheless, the overall outcome is clear, $\alpha1^{Mut}$ reduces cell surface
569 expression.

570 Given the reduced maximal GABA currents with the mutant receptors, we used flow
571 cytometry to study $GABA_AR$ expression efficiency. Flow cytometry corroborated the
572 electrophysiology findings revealing severely impaired cell surface trafficking for α1 mutant
573 receptors, with preferential co-expression with β3 over β2 subunits. A similar profile emerged
574 for receptor expression in neurons. The overall expression levels for WT and mutant α1
575 subunits (surface + intracellular) were identical in HEK-293 cells. The limited trafficking to
576 the cell surface occurred as a result of substantive retention in the ER. This may result from
577 the Lys373, in part, acting as a retention motif following truncation (Teasdale and Jackson,
578 1996).The 24 new amino acids contain two further Lys residues located at intervals of 7-8
579 residues, although these are not traditional retention motifs (Teasdale and Jackson, 1996).
580 Nevertheless, the outcome of ER retention is that the functionally-impaired α1 mutant is not
581 expressed on the cell surface efficiently, and this will be a major determining factor in
582 causing seizures as the efficacy of inhibition, imparted by the single WT allele, may not be
583 adequate to control neuronal excitation.

584 The addition of the 24 *de novo* amino acids after Lys373 had no impact on $GABA_AR$
585 signalling since there was no difference in GABA sensitivity or receptor kinetics between αβγ
586 receptors incorporating either $\alpha1^{Mut}$ or $\alpha1^{\Delta373}$. The additional amino acids had only a minimal
587 effect on cell surface expression of the mutant receptors as the truncation $\alpha1^{\Delta373}$ displayed a
588 slightly greater area in Q2 flow cytometry compared to $\alpha1^{Mut}$, a feature that is unlikely to be
589 significant for the seizure intensities observed in the individual harbouring the genetic
590 variant.

591 The first indication that $GABA_AR$ subunit composition may be affected by $\alpha1^{Mut}$ was evident
592 from the large amplitude reduction and increased decay kinetics for sIPSCs, which we

postulated may occur following incorporation of mutant subunits into synaptic $GABA_A$Rs. The reduced inhibitory transmission efficacy was not due to a dominant negative effect on the expression of other WT subunits as whole-cell maximal GABA-activated current densities were unaffected. A reduction in receptor numbers at inhibitory synapses could explain the reduction in sIPSC amplitudes. Impaired lateral diffusion-mediated recruitment/ retention of receptors at the synapse could also be due to the α1 subunit mutation, accounting for the changed synaptic current profiles. This concept also accords with the zolpidem effects on the sIPSC decays. Prolongation by zolpidem signals that α1-subunit $GABA_A$Rs are present at the inhibitory synapse, but this was clearly reduced by the presence of $\alpha1^{Mut}$. The simplest and also speculative explanation for this is that $\alpha1^{Mut}$ hinders the trafficking of the receptor to the synaptic membrane and could account for why sIPSC amplitudes are reduced whilst GABA whole-cell currents are unaffected, as $\alpha1^{Mut}$ receptors remain mostly outside the synapse. It was also notable that the control sIPSC decays for $\alpha1^{Mut}$ are longer than for $\alpha1^{WT}$ expressing neurons. This may signify an effect of $\alpha1^{Mut}$ on kinetics and/or the influx of other α subunit $GABA_A$Rs (e.g. α2) as part of a homeostatic mechanism.

As the mutant expression levels at the cell surface of transfected neurons equates to ~25% of WT subunit levels, but reduces sIPSC amplitudes by ~50%, suggested that a disproportionately larger pool of receptors contain mutant α1 subunits than expected. Furthermore, by modelling the concentration response curves for mixtures of two separate populations of $GABA_A$Rs containing either $\alpha1^{WT}$ or $\alpha1^{Mut}$ subunits, with varying expression levels, it became clear that the widely separated EC_{50}s for $\alpha1^{WT}$ and $\alpha1^{Mut}$ should be reflected by easily detected biphasic curves. This was not observed experimentally even though the curves for $\alpha1^{WT}$ (EC_{50} ~10 μM) and $\alpha1^{Mut}$ (EC_{50} 3.8 mM) are separated by an approximate 380-fold shift. The curve for a mixture of $\alpha1^{WT}$ and $\alpha1^{Mut}$ (EC_{50} 87 μM) was seemingly monophasic, which could not be accounted for by differential levels of α1 subunit expression, but could represent a heteromeric α subunit $GABA_A$R composed of both $\alpha1^{WT}$ and $\alpha1^{Mut}$. Using a binomial model for co-assembly does account for the GABA concentration response curve profiles but requires most (~95%) of the α1 subunit-containing receptors in the cell membrane to be either composed of $\alpha1^{WT}\beta3\gamma2L$ or $\alpha1^{WT}\alpha1^{Mut}\beta3\gamma2L$ receptors. This circumstance, whereby a pathological mutation readily assembles as part of a heteromeric α subunit $GABA_A$R complex can also be diversified to include a preference for β3 over β2 subunit assembly.

Thus, these new findings suggest that even though the structure and expression profile of mutant α1 subunits is significantly impaired, their low GABA sensitivity reduces the efficacy of synaptic inhibition of WT α1-containing $GABA_A$Rs by co-assembly in the same pentamer.

628 This heteromeric co-assembly not only adds an additional level of complexity to epilepsy-
629 causing haploinsufficiency, but also presents the likelihood that selected heteromeric (WT) α
630 subunit receptors may be physiologically more prevalent in the brain than previously thought,
631 adding to the structural diversity of neuronal $GABA_AR$s.

632

633 **Figure Legends**

634 **Fig. 1.** Severe reduction in the GABA sensitivity of mutant α1-$GABA_A$Rs.

635 *(A)* Schematic showing the location of the α1-$GABA_A$R variant in the M3-M4 loop with and
636 without the additional 24 amino acids. *(B)* GABA-activated currents for WT and mutant α1
637 subunits expressed with β3γ2L in HEK-293 cells. *(C)* GABA concentration response
638 relationships for WT and α1 mutant receptors. Insets: GABA EC_{50}s and normalised maximal
639 GABA currents. *(D)* Averaged currents evoked by saturating GABA (1 mM WT, 100 mM
640 mutants). Examples of activation and deactivation of GABA currents are shown together with
641 averaged activation and deactivation rates. Activation rate was calculated by measuring the
642 time taken to ascend from 20 to 80% of maximal current following the application of GABA.
643 Deactivation rate was calculated by exponential fitting to the current decay immediately after
644 cessation of GABA application. NS – not significant, *P<0.05, **P<0.01, ***P<0.001, One-
645 way ANOVA.

646

647 **Fig. 2.** Reduced sensitivity to GABA for α1 mutants expressed in *Xenopus* oocytes.

648 *(A)* Representative GABA-activated currents for wild-type and mutant receptors expressed in
649 *Xenopus* oocytes with β2γ2L or β3γ2L. *(B)* GABA concentration response relationships for
650 wild-type and α1 mutant receptors. *(C)* GABA EC_{50}s for α1β2γ2L (n = 7); $α1^{Mut}$β2γ2L (n = 5);
651 α1β3γ2L (n = 8); and $α1^{Mut}$β3γ2L (n = 5). *(D)* Maximum GABA-activated currents for wild-
652 type and mutant α1 receptors. The maximal GABA concentration applied was 100 mM.
653 Normalised maximal currents (to wild-type) shown for α1β2γ2L (n = 7); $α1^{Mut}$β2γ2L (n = 8);
654 α1β3γ2L (n = 7); and $α1^{Mut}$β3γ2L (n = 5). *P<0.05, **P<0.01, ***P<0.001 two-tailed unpaired
655 t test.

656

657 **Fig. 3.** Impaired cell surface expression of α1 mutant $GABA_A$Rs in HEK-293 cells.

658 *(A)* Cytofluorograms for cell surface α1 WT and mutant $GABA_A$Rs in HEK-293 cells
659 expressed with either β2γ2L (top line) or β3γ2L (bottom) subunits. The numbers in
660 quadrants (Q) 1-4) show percentages of detected cells. *(B, C)* Left panel, normalised (Norm.;
661 %) median cell surface fluorescence (F) for: *B*, $α1^{x}$β2γ2L and *C,* $α1^{x}$β3γ2L (where x = WT,
662 Mut or Δ373), including eGFP and untransfected (untrans.) controls in Q2. Right panel,
663 mean % number of expressing cells in Q2 for $α1^{x}$β2γ2L (*B*) and $α1^{x}$β3γ2L (*C*). Non-

normalised data-points are shown by symbols superimposed on the bar charts with the right-hand ordinate denoting their values. au – arbitrary units. *(D)* Cytofluorograms for total (intracellular and surface) α1 WT and mutant receptors in permeabilised HEK-293 cells expressing β2γ2L or β3γ2L. *(E and F)* Left panels, median (%) total fluorescence for $\alpha1^{x}\beta2\gamma2L$ (*E*) and $\alpha1^{x}\beta3\gamma2L$ (*F*). Right panels, % cells in Q2 expressing $\alpha1^{x}\beta2\gamma2L$ (*E*) and $\alpha1^{x}\beta3\gamma2L$ (*F*). All data are normalised to the WT data. NS – not significant, **P<0.01, ***P<0.001, One-way ANOVA. n = 5 - 7 independent experiments with 25000-50000 cells per construct per run.

Fig. 4. Effect of an assembly box sequence on cell surface expression and expression of α1-$GABA_A$Rs in hippocampal neurons.

(A) Cytofluorograms for cell surface α1 WT and mutant $GABA_A$Rs in HEK-293 cells expressed with either β3γ2L or $\beta3^{DNTK}\gamma2L$ subunits. *(B)* Normalised (Norm.) mean % number of expressing cells in Q2 for α1 with β3γ2L or $\beta3^{DNTK}\gamma2L$. Non-normalised data-points are shown (symbols) on each bar chart with values denoted by the right-hand ordinate. *P<0.05, ***P<0.001, One-way ANOVA. n = 3 independent experiments with 25000-50000 cells per construct per run. *(C)* Representative GABA-activated currents for untagged and myc-tagged wild-type α1 subunit receptors expressed in HEK-293 cells with β2γ2L subunits to check functional neutrality of the myc-tag. *(D)* GABA concentration response relationships for untagged or myc-tagged WT α1β2γ2L receptors. EC_{50s} - α1β2γ2L, 7.2 ± 1 μM, n = 8; $\alpha1^{myc}\beta2\gamma2L$, 7.5 ± 1.2 μM, n = 6. *(E)* Confocal images of hippocampal cell surface labelling showing myc-tagged WT or mutant α1-containing $GABA_A$Rs (left column), eGFP staining (middle), and merged images of α1 and GFP fluorescence (right). Calibration bars = 5 μm. *(F)* Mean fluorescence intensities for WT and mutant α1-containing $GABA_A$R cell surface labelling in neurons. au – arbitrary units. **P<0.01, ***P<0.001, One-way ANOVA, n = 36.

Fig. 5. Intracellular retention of mutant $GABA_A$Rs in the endoplasmic reticulum.

(A) Representative confocal images of wild-type and mutant α1-containing $GABA_A$Rs expressed in HEK-293 cells. The left column (from the top) shows rows for cells expressing: GFP or α1 subunits only; $\alpha1^{Mut}$ with either β2 or β3 and γ2L; and $\alpha1^{WT}$ with either β2 or β3 and γ2L subunits. The middle column depicts immunostains for the ER-associated protein, calnexin, and the right hand column exhibits the extent of co-localisation for $\alpha1^{WT}$ and $\alpha1^{Mut}$

subunits with calnexin. Note that the images are represented as pseudo-colours. *(B)* Bargraphs report Pearson's correlation coefficient (r), and Mander's M1/2 coefficients also measuring co-localisation of α1 and calnexin. M1 reports α1 co-localised with calnexin, and M2 denotes calnexin co-localised with α1 subunits. *P<0.05, **P<0.01, ***P<0.001, One-way ANOVA, n = 18-28. Scale bar 5 μm.

Fig. 6. Mutant α1 subunit-$GABA_A$Rs reduce sIPSC amplitudes.

(A) Top panel, sIPSCs recorded from cultured hippocampal neurons clamped at -60 mV and expressing WT or mutant α1-containing $GABA_A$Rs. Higher time resolution records from selected panels (dotted lines) are shown below. *(B)* From left to right: averaged sIPSC waveforms; sIPSC frequency and cumulative probability distribution of sIPSC amplitudes (inset: box plot showing median and 25-75% interquartile range (IQR) of amplitudes (Amp.)); sIPSC half-decay time (T_{50}), exponential decay times and cumulative distribution of area (charge transfer) (inset: box plot shows median and 25-75% IQR of the sIPSC area), for WT and mutant α1 subunit-containing $GABA_A$Rs. NS – not significant, **P<0.01, two-tailed unpaired t test, n = 21-25 neurons for bar charts. ***P<0.001, Mann-Whitney test. n = 5236 – 5664 events for sIPSC cumulative amplitude distributions from 24-25 cells. n = 1306-1330 for sIPSC cumulative area distributions. *(C)* Whole-cell 1 mM GABA-activated currents recorded at -20 mV in neurons expressing $\alpha1^{WT}$ or $\alpha1^{Mut}$ $GABA_A$Rs. *(D)* Mean GABA current densities for $\alpha1^{WT}$- and $\alpha1^{Mut}$-expressing neurons (n = 41 - 45 neurons). NS – not significant, two-tailed unpaired t test. *(E)* Non-stationary noise analysis for sIPSCs recorded from neurons expressing WT or mutant $GABA_A$Rs. *(F)* Bargraphs of number of receptors (N) at inhibitory synapses activated during the peak sIPSC, and single channel conductance (G), of $GABA_A$Rs. n = 9 – 11 neurons; *P<0.05, two-tailed unpaired t test.

Fig. 7. Formation of α1-heteromeric $GABA_A$Rs

(A) GABA-activated currents for pure and mixed α1 subunit-containing receptors expressed with β3γ2L in HEK-293 cells. *(B)* EC_{50} values are plotted for individual cells for pure and mixed α1 subunit-containing receptors. Arbitrarily defined type 1 receptors have EC_{50}s similar to wild-type and type 2 receptors have ~8-fold higher EC_{50}s. *(C)* GABA concentration response relationships for α1 WT and for cells expressing $\alpha1^{Mut}$ with α1 WT subunits n = 41 for type 1 receptors, 5 for type 2 receptors and 14 for wild-type receptors. The curve for

$\alpha1^{Mut}\beta3\gamma2L$ is shown for comparison (orange dashed line), data taken from Fig. 1*C*. *(D)* GABA concentration curves generated by a modified Hill equation based on expressing just two pure populations of receptors: $\alpha1^{WT}\beta3\gamma2L$ and $\alpha1^{Mut}\beta3\gamma2L$ with EC_{50}s from Fig. 1*C*. Note as $\alpha1^{Mut}$ receptors were trafficking-impaired, their access to the cell surface was limited to 10 % of WT. The relative proportions (%) of $\alpha1^{WT}$ and $\alpha1^{Mut}$ were varied between curves from 100 ($\alpha1^{WT}$):0 ($\alpha1^{Mut}$)% (black line), to 50:50 and 10:90 (green), and 0:100 (orange dashed line). *(E)* Simulated GABA concentration response curves for a binomial mixture of $\alpha1^{WT}$ and $\alpha1^{Mut}$ with β3 and γ2L subunits as indicated by the key. A binomial distribution was assumed to occur for assembly ($\alpha1^{WT}$ 25%, $\alpha1^{WT}\alpha1^{Mut}$ 50%, $\alpha1^{Mut}$ 25%) with trafficking to the cell surface as ($\alpha1^{WT}$ 54%, $\alpha1^{WT}\alpha1^{Mut}$ 40% and $\alpha1^{Mut}$ 6%) with EC_{50}s and Hill slopes of ($\alpha1^{WT}$ 6.93 μM, 1.33; $\alpha1^{WT}\alpha1^{Mut}$ 87 μM, 0.79 (type 2 blue curve), 3.58μM, 1.63 (type 1, red curve); $\alpha1^{Mut}$ 10.7 mM, 0.56).

Fig. 8. Expression of the α1 mutant subunits does not affect α1 subunit surface expression and potentiation of IPSCs by zolpidem.

(A) Confocal images of cell surface labelling of WT $\alpha1^{myc}$ $GABA_A$Rs in the absence (top row) or presence of co-expressed mutant α1 or eGFP only. Calibration bars = 5 μm. *(B)* Mean fluorescence intensities for WT α1 $GABA_A$Rs in the absence and presence of mutant α1 or eGFP only. Data normalised to levels of $\alpha1^{WT}$ myc staining. NS – not significant, One-way ANOVA, n = 24 - 42. *(C)* Representative sIPSCs recorded from hippocampal neurons expressing $\alpha1^{WT}$ or mutant $\alpha1^{Mut}$-containing $GABA_A$Rs under control conditions or in the presence of 100 nM zolpidem. *(D, E)* Average sIPSC waveforms, half-decay times (T_{50}) and decay τ in the presence of 100 nM zolpidem for $\alpha1^{WT}$ (*D*) and $\alpha1^{Mut}$ (*E*) expressing neurons. n = 9 - 12, **P<0.01, ***P<0.001; two-tailed paired t test.

Table 1 – Mean EC_{50}s, maximal GABA-activated currents, activation and deactivation rates for GABA currents mediated by mutant and wild-type α1 subunit receptors expressed in HEK-293 cells with β and γ2L subunits.

HEK Cells	EC_{50}	S.E.M	Units	N (cells)	N (trials)	Average Hill Slope	P	Fig
α1β3γ2L	8.8	1.7	μm	6	3	1.2 ± 0.1	| ** | * | NS	1C
$α1^{Lys373Serfs*25}$β3γ2L	3798	704	μm	7	3	0.6 ± 0.03		
$α1^{Δ373}$β3γ2L	3406	999	μm	6	2	0.6 ± 0.04		
	I Max	S.E.M	Units	N (cells)	N (trials)		P	Fig
α1β3γ2L	100	-		11	3		| *** | *** | NS	1C
$α1^{Lys373Serfs*25}$β3γ2L	11.1	2.9	% control	7	3			
$α1^{Δ373}$β3γ2L	9.4	1	% control	8	3			

	Activation Rate	S.E.M	Units	N (cells)	N (trials)	P	Fig
α1β3γ2L	0.036	0.004	s	8	2	| ** | * | NS	1D
$α1^{Lys373Serfs*25}$β3γ2L	0.22	0.05	s	9	2		
$α1^{Δ373}$β3γ2L	0.17	0.03	s	7	2		
	Deactivation τ	S.E.M	Units	N (cells)	N (trials)	P	Fig
α1β3γ2L	0.2	0.02	τ (s)	5	2	| * | * | NS	1D
$α1^{Lys373Serfs*25}$β3γ2L	0.56	0.08	τ (s)	10	2		
$α1^{Δ373}$β3γ2L	0.51	0.08	τ (s)	9	2		

S.E.M – standard error of mean, NS – not significant, *P<0.05, **P<0.01, ***P<0.001; One-way ANOVA

Table 2 – Mean cell surface fluorescence and % area Q2 of flow cytometry

	Mean Normalised Median surface fluorescence	S.E.M	N (trials)	Fig
α1β2γ2L	100	-	7	3B
$\alpha1^{Lys373Serfs*25}$β2γ2L	60.9	9.5	7	
$\alpha1^{\Delta373}$β2γ2L	47.7	7.2	5	
Untransfected	0	0	7	
eGFP control	0	0	7	
	Mean Normalised Median surface fluorescence	S.E.M	N (trials)	Fig
α1β3γ2L	100	-	6	3C
$\alpha1^{Lys373Serfs*25}$β3γ2L	29.2	6.3	6	
$\alpha1^{\Delta373}$β3γ2L	32.1	6.7	5	
Untransfected	0	0	6	
eGFP control	0	0	6	
	Mean Normalised Median intracellular fluorescence	S.E.M	N (trials)	Fig
α1β2γ2L	100	-	5	3E
$\alpha1^{Lys373Serfs*25}$β2γ2L	86.3	6.7	5	
Untransfected	0	0	5	
eGFP control	0	0	5	
	Mean Normalised Median intracellular fluorescence	S.E.M	N (trials)	Fig
α1β3γ2L	100	-	5	3F
$\alpha1^{Lys373Serfs*25}$β3γ2L	89.2	8.4	5	
Untransfected	0	0	5	
eGFP control	0	0	5	
	Mean Normalised surface Q2 Area	S.E.M	N (trials)	Fig
α1β2γ2L	100	-	7	3B
$\alpha1^{Lys373Serfs*25}$β2γ2L	6.1	1.6	7	
$\alpha1^{\Delta373}$β2γ2L	5.2	1.1	5	
Untransfected	0	0	7	
eGFP control	0	0	7	
	Mean Normalised surface Q2 Area	S.E.M	N (trials)	Fig
α1β3γ2L	100	-	6	3C
$\alpha1^{Lys373Serfs*25}$β3γ2L	24.7	4.3	6	
$\alpha1^{\Delta373}$β3γ2L	39.8	3.2	5	
Untransfected	0	0	6	
eGFP control	0	0	6	
	Mean Normalised intracellular Q2 Area	S.E.M	N (trials)	Fig
α1β2γ2L	100	-	5	3E
$\alpha1^{Lys373Serfs*25}$β2γ2L	84.1	14.5	5	
Untransfected	0	3.2	5	
eGFP control	0	0	5	
	Mean Normalised intracellular Q2 Area	S.E.M	N (trials)	Fig
α1β3γ2L	100	-	5	3F
$\alpha1^{Lys373Serfs*25}$β3γ2L	121	27	5	
Untransfected	0	0	5	
eGFP control	0	0	5	
	Mean Normalised surface Q2 Area	S.E.M	N (trials)	Fig
α1β3γ2L	100	-	3	4B
$\alpha1^{Lys373Serfs*25}$β3γ2L	33.1	3	3	
$\alpha1^{Lys373Serfs*25}$$\beta3^{DNTK}$γ2L	19.9	4.2	3	
Untransfected	0.1	0.03	3	
eGFP control	0	0	3	

S.E.M – standard error of mean

Author contributions

SH conceived the project. SH, AHBA, PG, GW designed and carried out the flow cytometry experiments. SH and CJ performed the electrophysiology. SH, MM carried out the imaging experiments. TGS performed the theoretical GABA concentration response relationship analyses. BP, RT analysed patient data. SH, DN and TGS supervised the project. SH and TGS wrote the manuscript and all authors contributed to the writing.

References

Audenaert D, Schwartz E, Claeys KG, Claes L, Deprez L, Suls A, Van DT, Lagae L, Van BC, MacDonald RL, De Jonghe P (2006) A novel *GABRG2* mutation associated with febrile seizures. Neurology 67:687–690.

Connolly CN, Krishek BJ, McDonald BJ, Smart TG, Moss SJ (1996) Assembly and cell surface expression of heteromeric and homomeric γ-aminobutyric acid type-A receptors. J Biol Chem 271:89–96.

Datta D, Arion D, Lewis DA (2015) Developmental Expression Patterns of $GABA_A$ Receptor Subunits in Layer 3 and 5 Pyramidal Cells of Monkey Prefrontal Cortex. Cereb Cortex Cereb Cortex 25:2295-2305.

Fisher JL (2004) A mutation in the $GABA_A$ receptor α1 subunit linked to human epilepsy affects channel gating properties. Neuropharmacology 46:629-637.

Foo JN, Liu JJ, Tan EK (2012) Whole-genome and whole-exome sequencing in neurological diseases. Nat Rev Neurol. 8:508-517.

Galanopoulou A (2010) Mutations affecting GABAergic signaling in seizures and epilepsy. Pflugers Arch Eur J Physiol 460:505–523.

Gallagher MJ, Shen W, Song L, Macdonald RL (2005) Endoplasmic reticulum retention and associated degradation of a $GABA_A$ receptor epilepsy mutation that inserts an aspartate in the M3 transmembrane segment of the α1 subunit. J Biol Chem 280:37995-38004.

Hales TG, Tang H, Bollan KA, Johnson SJ, King DP, McDonald NA, Cheng A, Connolly CN (2005) The epilepsy mutation, γ2 (R43Q) disrupts a highly conserved inter-subunit contact site, perturbing the biogenesis of $GABA_A$ receptors. Mol Cell Neurosci 29:120-127.

Hannan S, Minere M, Harris J, Izquierdo P, Thomas P, Tench B, Smart TG (2019) $GABA_AR$ isoform and subunit structural motifs determine synaptic and extrasynaptic receptor localisation. Neuropharmacology 107540. doi: 10.1016/j.neuropharm.2019.02.022.

Hannan S, Smart TG (2018) Cell surface expression of homomeric $GABA_A$ receptors depends on single residues in subunit transmembrane domains. J Biol Chem 293:13427–13439.

Hannan S, Wilkins ME, Thomas P, Smart TG (2013) Tracking cell surface mobility of GPCRs using α-bungarotoxin-linked fluorophores. Methods Enzym 521:109–129.

Hanrahan JW (2004) Cystic fibrosis transmembrane conductance regulator. Adv Mol Cell Biol. 32:73-94.

816 Hernandez CC, Klassen TL, Jackson LG, Gurba K, Hu N, Noebels JL, Macdonald RL (2016)
817 Deleterious rare variants reveal risk for loss of $GABA_A$ receptor function in patients with
818 genetic epilepsy and in the general population. PLoS One 11:e0162883.

819 Hutcheon B, Fritschy JM, Poulter MO (2004) Organization of GABA receptor α-subunit 26
820 clustering in the developing rat neocortex and hippocampus. Eur J Neurosci 19:2475–
821 2487.

822 Jansen M, Bali M, Akabas MH (2008) Modular Design of Cys-loop Ligand-gated Ion
823 Channels: Functional 5-HT_3 and GABA ρ1 Receptors Lacking the Large Cytoplasmic
824 M3-M4 Loop. J Gen Physiol 131:137–146.

825 Kang J-QJ, Macdonald RL (2004) The $GABA_A$ receptor γ2 subunit R43Q mutation linked to
826 childhood absence epilepsy and febrile seizures causes retention of α1β2γ2S receptors
827 in the endoplasmic reticulum. J Neurosci 24: 8672–8677.

828 Kang JQ, Macdonald RL (2009) Making sense of nonsense $GABA_A$ receptor mutations
829 associated with genetic epilepsies. Trends Mol Med 15:430–438.

830 Kang JQ, Shen W, Macdonald RL (2009) The *GABRG2* Mutation, Q351X, Associated with
831 Generalized Epilepsy with Febrile Seizures Plus, Has Both Loss of Function and
832 Dominant-Negative Suppression. J Neurosci 29:2845–2856.

833 Kang JQ, Shen W, Zhou C, Xu D, Macdonald RL (2015) The human epilepsy mutation
834 *GABRG2* (Q390X) causes chronic subunit accumulation and neurodegeneration. Nat
835 Neurosci 18:988-996.

836 Lachance-Touchette P, Brown P, Meloche C, Kinirons P, Lapointe L, Lacasse H, Lortie A,
837 Carmant L, Bedford F, Bowie D, Cossette P (2011) Novel α1 and γ2 $GABA_A$ receptor
838 subunit mutations in families with idiopathic generalized epilepsy. Eur J Neurosci
839 34:237-249.

840 Leach MR, Williams DB (2011) Calnexin and Calreticulin, Molecular Chaperones of the
841 Endoplasmic Reticulum. In: Eggleton P., Michalak M. (eds) Calreticulin. Molecular
842 Biology Intelligence Unit. Springer, Boston, MA.

843 MacDonald RL, Gallagher MJ, Feng HJ, Kang J (2004) $GABA_A$ receptor epilepsy mutations.
844 Biochem Pharmacol 68:1497–1506.

845 Maljevic S, Krampfl K, Cobilanschi J, Tilgen N, Beyer S, Weber YG, Schlesinger F, Ursu D,
846 Melzer W, Cossette P, Bufler J, Lerche H, Heils A (2006) A mutation in the $GABA_A$
847 receptor α1-subunit is associated with absence epilepsy. Ann Neurol. 59:983-987.

848 Maljevic S, Møller RS, Reid CA, Pérez-Palma E, Lal D, May P, Lerche H (2019) Spectrum of
849 $GABA_A$ receptor variants in epilepsy. Curr Opin Neurol. 32:183-190.

850 Mann EO, Paulsen O (2007) Role of GABAergic inhibition in hippocampal network
851 oscillations. Trends Neurosci 30:343–349.

852 Mitchell SJ, Silver RA (2003) Shunting inhibition modulates neuronal gain during synaptic
853 excitation. Neuron 38:433–445.

854 Perrais D, Ropert N (1999) Effect of zolpidem on miniature IPSCs and occupancy of
855 postsynaptic $GABA_A$ receptors in central synapses. J Neurosci 19:578–588.

856 Popp B, Trollmann R, Büttner C, Caliebe A, Thiel CT, Hüffmeier U, Reis A, Zweier C (2016)
857 Do the exome: A case of Williams-Beuren syndrome with severe epilepsy due to a
858 truncating de novo variant in *GABRA1*. Eur J Med Genet 59:549-553.

859 Pritchett DB, Lüddens H, Seeburg PH (1989) Type I and type II $GABA_A$-benzodiazepine
860 receptors produced in transfected cells. Science 245:1389-1392.

861 Robinson R, Gardiner M (2000) Genetics of childhood epilepsy. Arch Dis Child. 82:121–125.

862 Sancar F, Czajkowski C (2004) A $GABA_A$ receptor mutation linked to human epilepsy
863 (γ2R43Q) impairs cell surface expression of αβγ receptors. J Biol Chem 279, 47034-
864 47039.

865 Sieghart W, Sperk G (2002) Subunit composition, distribution and function of $GABA_A$
866 receptor subtypes. Curr Top Med Chem 2:795–816.

867 Sigel E, Steinmann ME (2012) Structure, Function, and Modulation of $GABA_A$ Receptors. J
868 Biol Chem 287:40224–40231.

869 Smart TG, Krishek BJ (2003) Xenopus Oocyte Microinjection and Ion-Channel Expression.
870 In: Patch-Clamp Applications and Protocols (Boulton AA, Baker GB, Walz W, eds).

871 Taylor PM, Connolly CN, Kittler JT, Gorrie GH, Hosie A, Smart TG, Moss SJ (2000)
872 Identification of residues within $GABA_A$ receptor α subunits that mediate specific
873 assembly with receptor β subunits. J Neurosci 20:1297–1306.

874 Taylor PM, Thomas P, Gorrie GH, Connolly CN, Smart TG, Moss SJ (1999) Identification of
875 amino acid residues within $GABA_A$ receptor β subunits that mediate both homomeric
876 and heteromeric receptor expression. J Neurosci 19:6360-6371.

877 Teasdale RD, Jackson MR (1996) Signal-mediated sorting of membrane proteins between
878 the endoplasmic reticulum and the golgi apparatus. Annu Rev Cell Dev Biol. 12:27-54.

879 Thomas P, Smart TG (2012) Use of electrophysiological methods in the study of
880 recombinant and native neuronal ligand-gated ion channels in the Study of
881 Recombinant and Native Neuronal Ligand-Gated Ion Channels. Curr Protoc Pharmacol.
882 59: 11.4.1-11.4.37.

883 Tian M, Mei D, Freri E, Hernandez CC, Granata T, Shen W, Macdonald RL, Guerrini R
884 (2013) Impaired surface αβγ $GABA_A$ receptor expression in familial epilepsy due to a
885 *GABRG2* frameshift mutation. Neurobiol Dis 50:135–141.

886 Vicini S, Ferguson C, Prybylowski K, Kralic J, Morrow AL, Homanics GE (2001) $GABA_A$
887 receptor α1 subunit deletion prevents developmental changes of inhibitory synaptic
888 currents in cerebellar neurons. J Neurosci 21:3009–3016.

889 Whiting PJ (2003) $GABA_A$ receptor subtypes in the brain: A paradigm for CNS drug
890 discovery? Drug Discov Today 8:445-450.

891

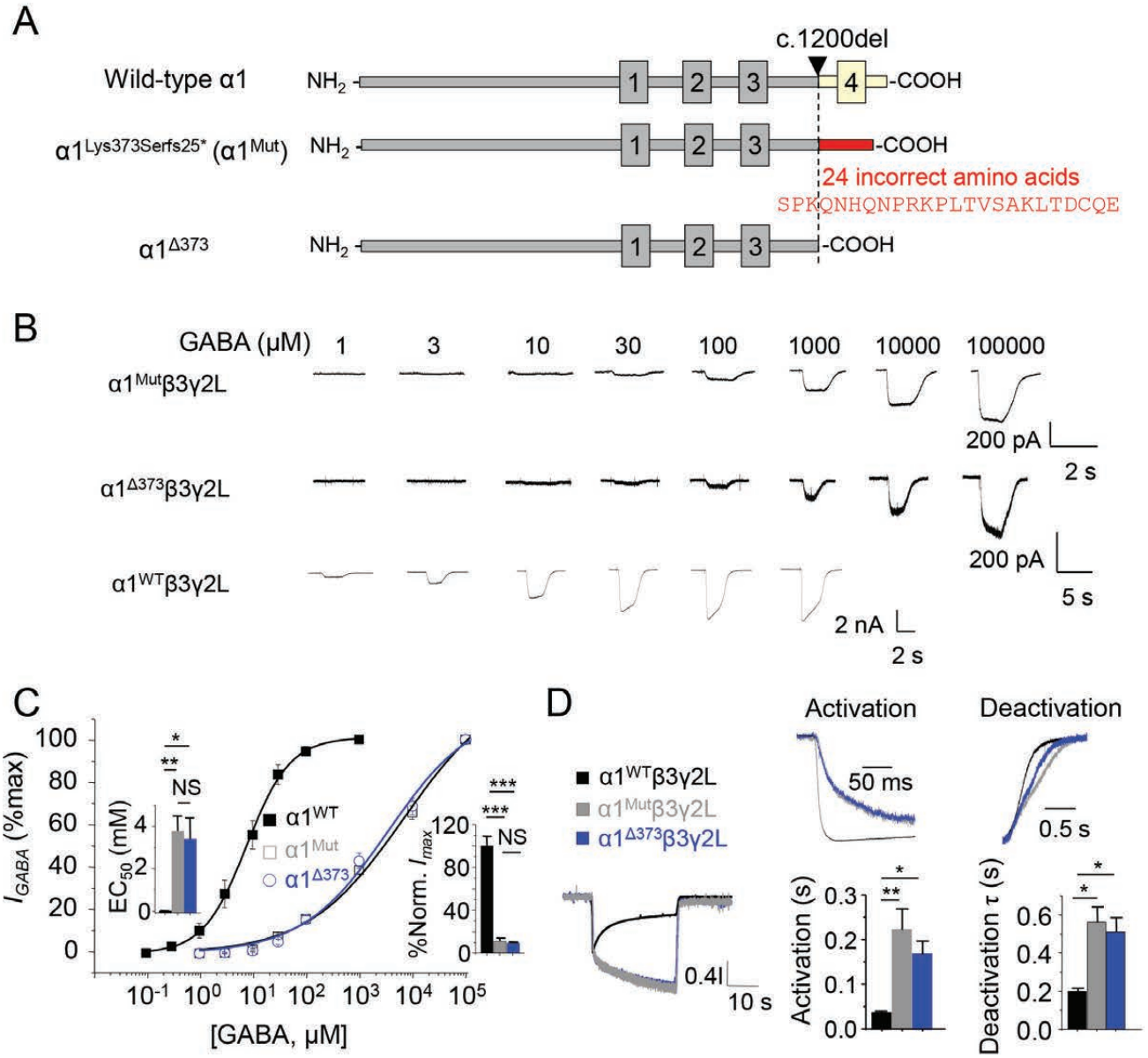

Figure 1

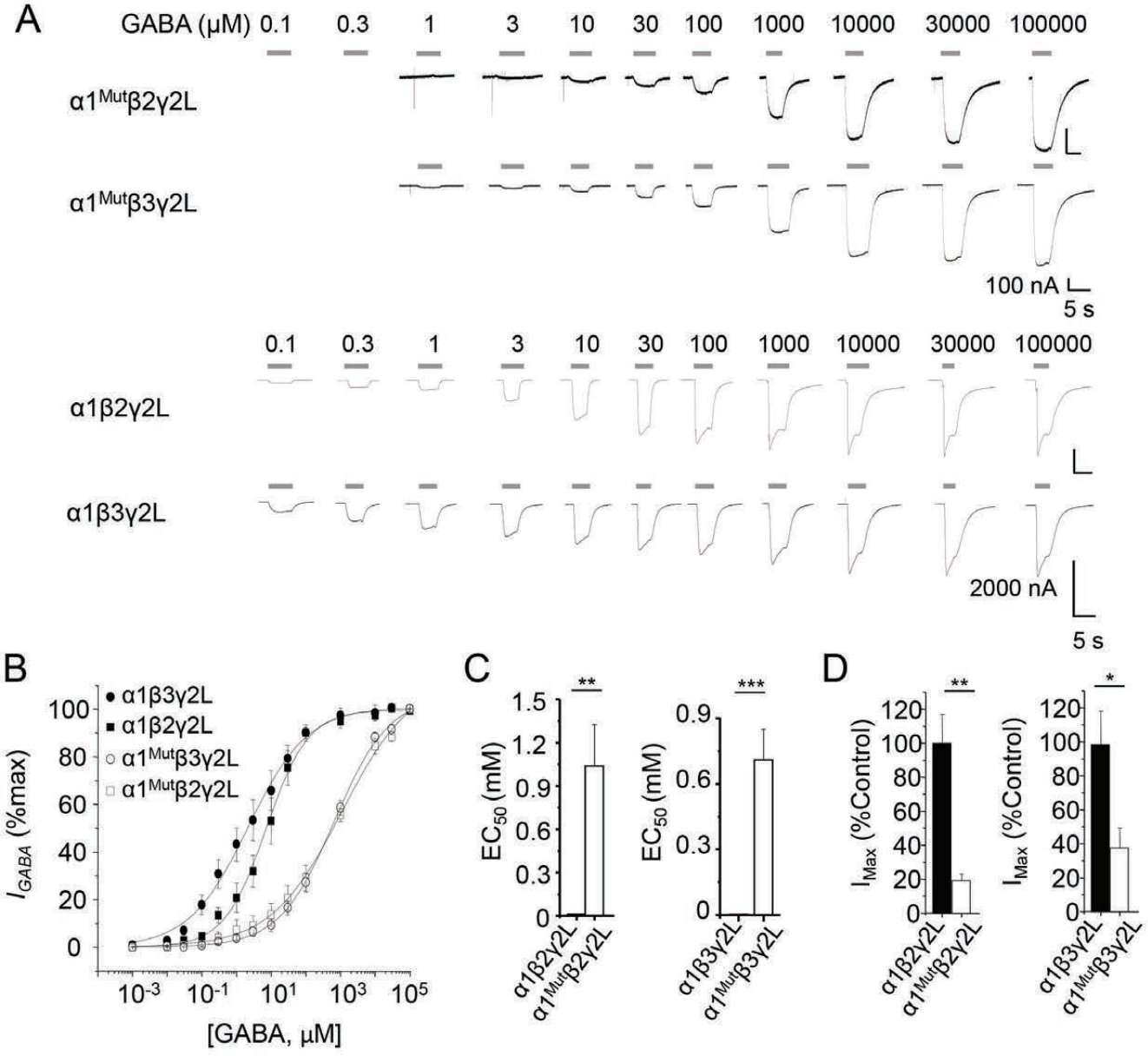

Figure 2

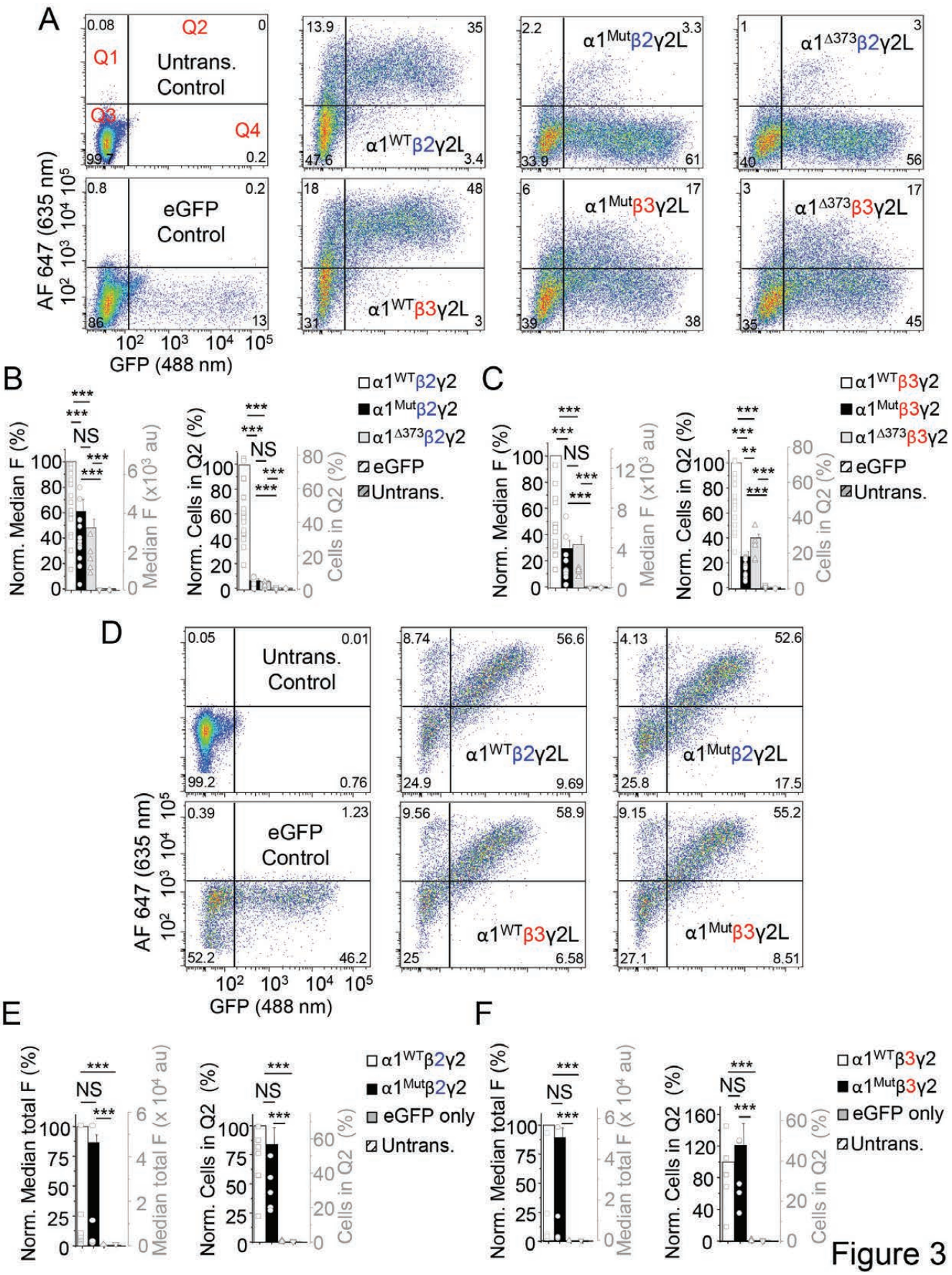

Figure 3

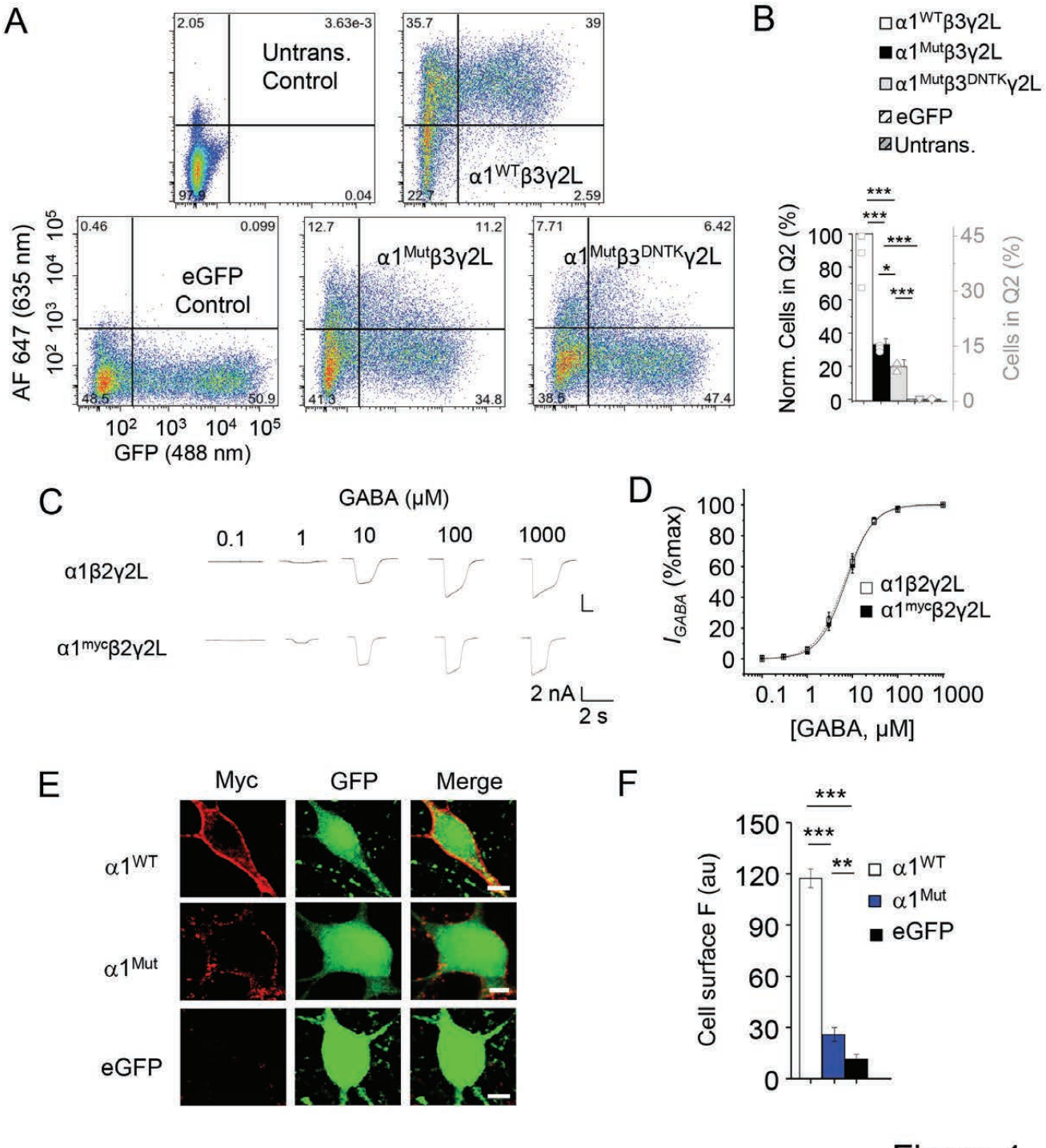

Figure 4

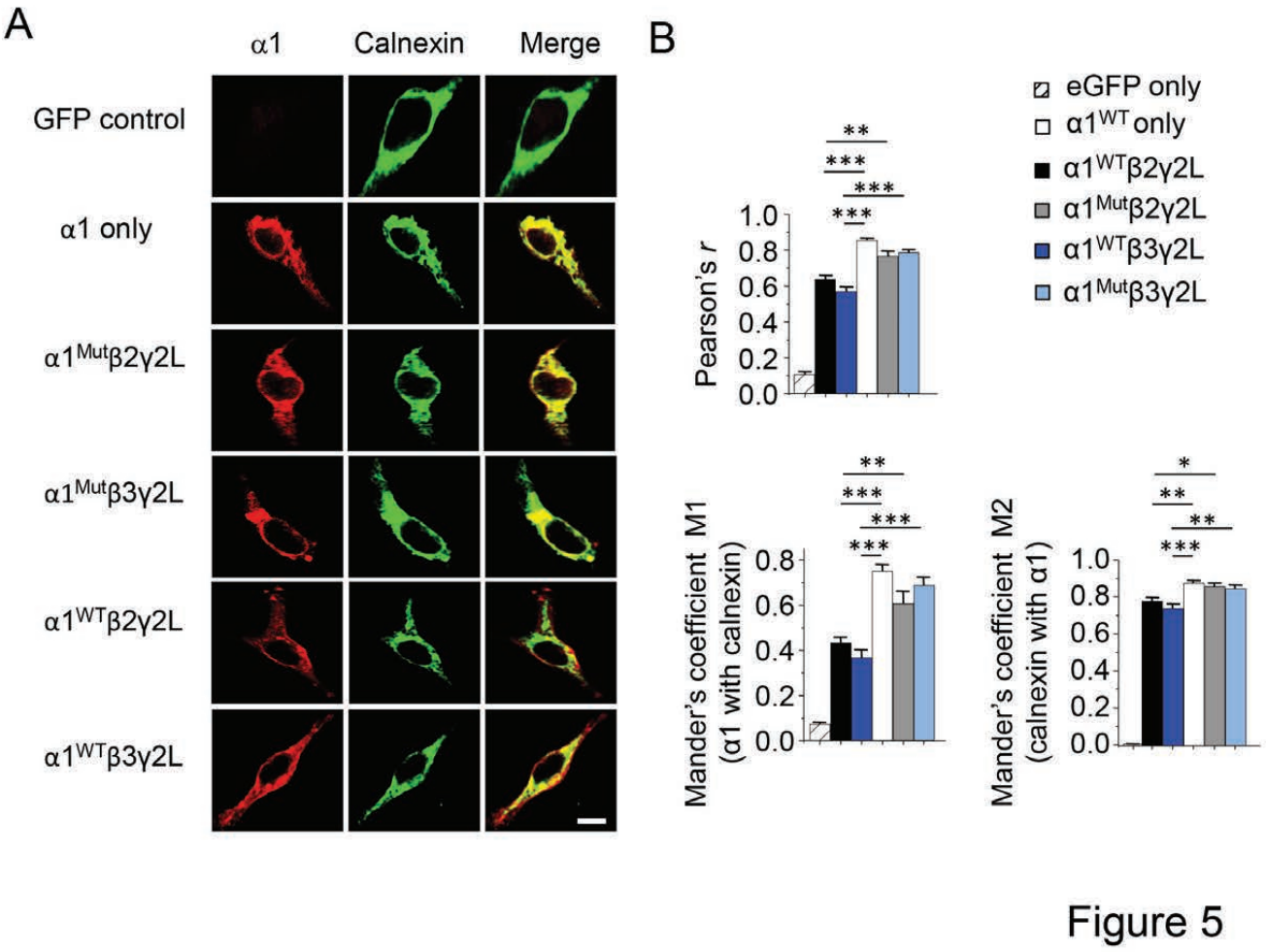

Figure 5

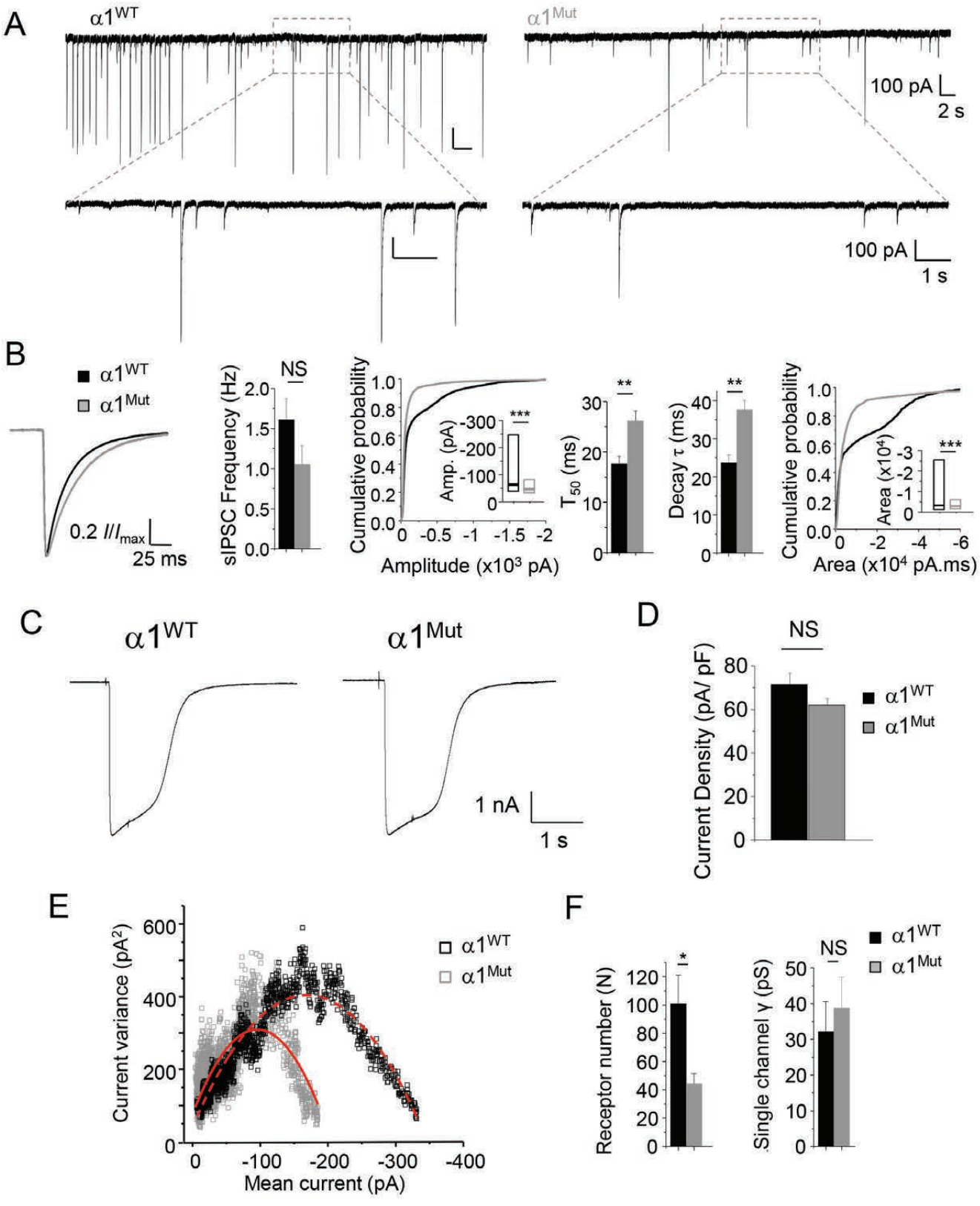

Figure 6

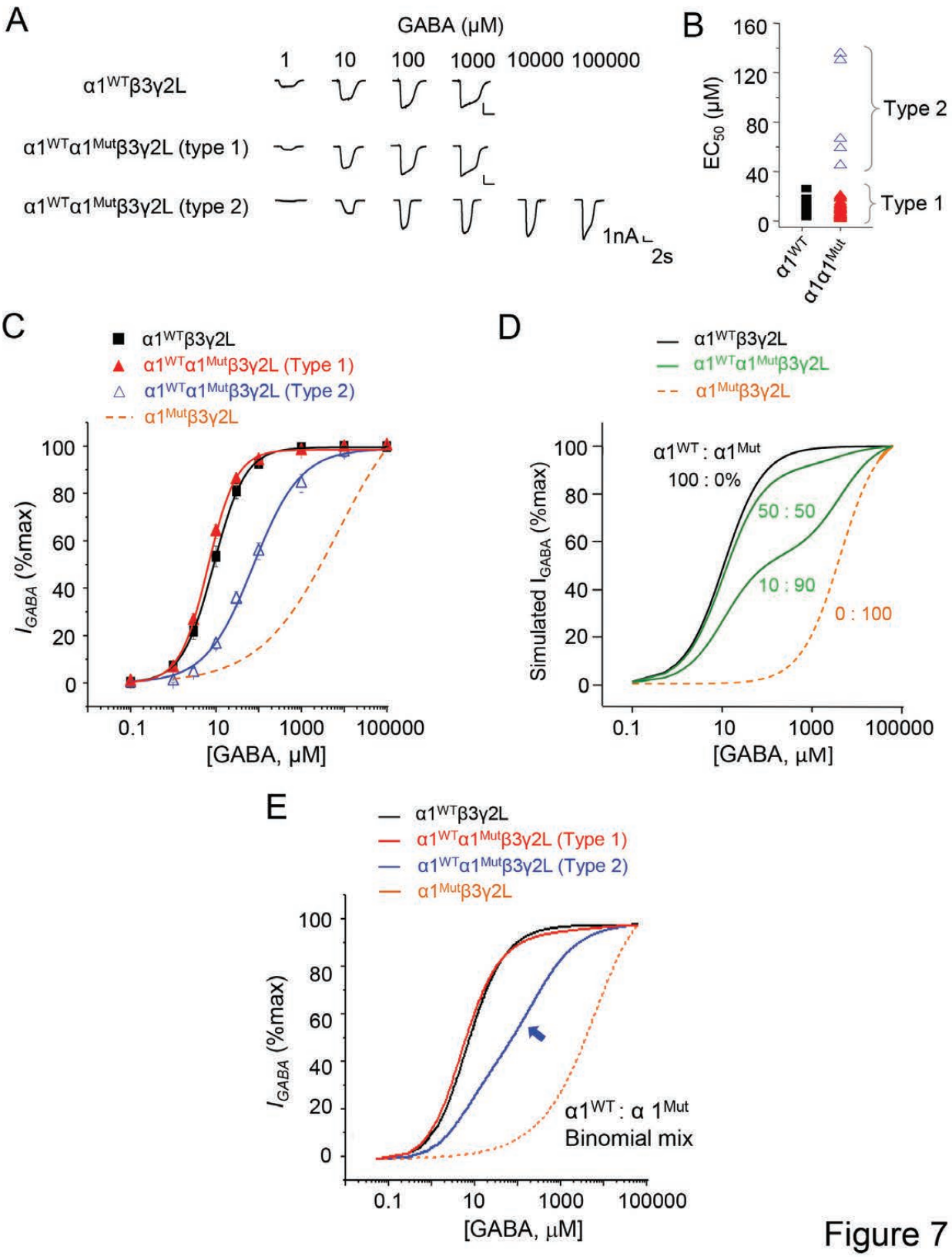

Figure 7

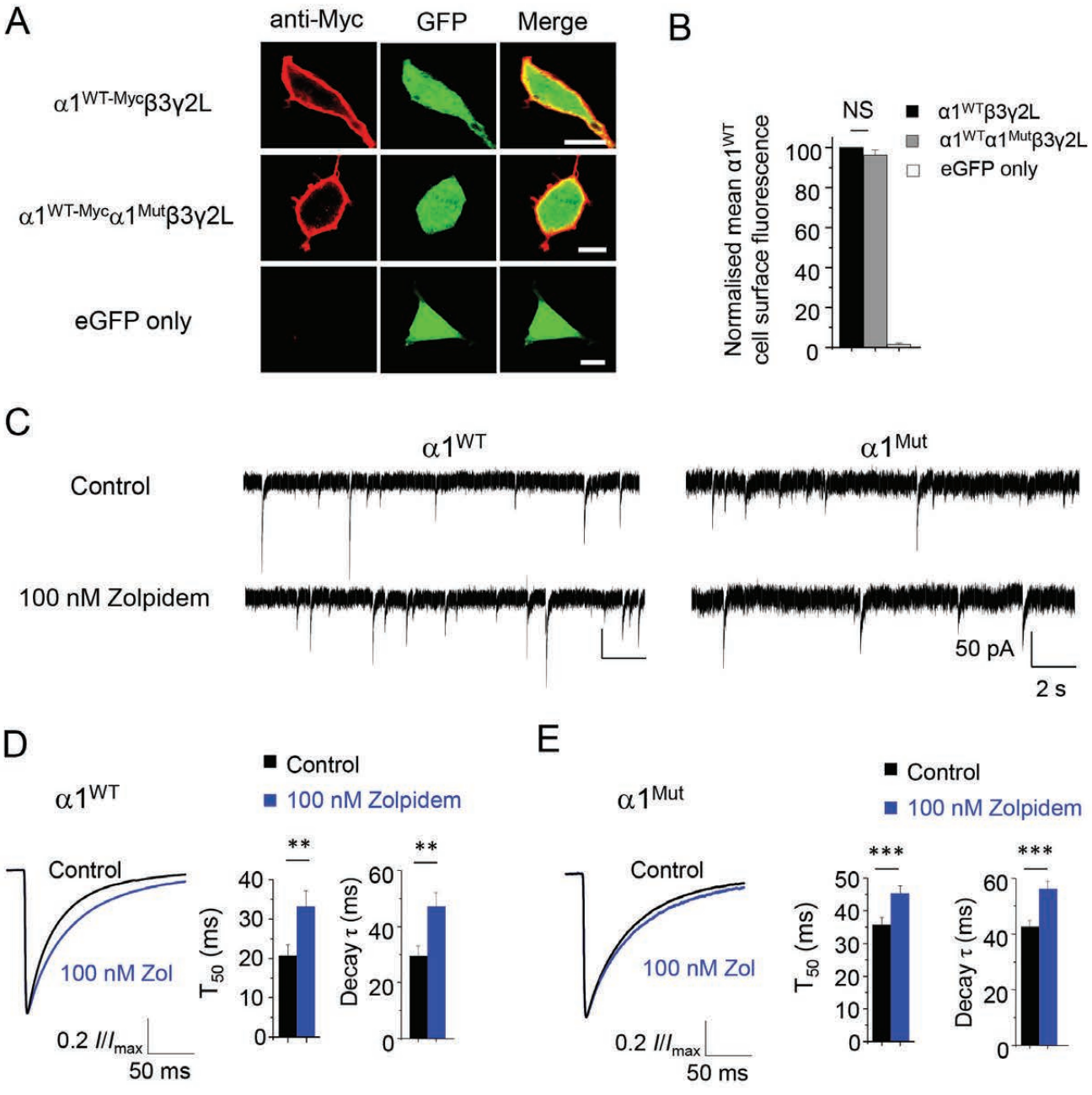

Figure 8